TRIM14 is a key regulator of the type I interferon response during *Mycobacterium tuberculosis* infection

Caitlyn T. Hoffpauir[1], Samantha L. Bell[1], Kelsi O. West[1], Tao Jing[2], Sylvia Torres-Odio[1], Jeffery S. Cox[3], A. Phillip West[1], Pingwei Li[2], Kristin L. Patrick[1], Robert O. Watson[1]

[1]Department of Microbial Pathogenesis and Immunology, Texas A&M Health Science Center, Bryan, TX 77807, USA

[2]Department of Biochemistry and Biophysics, Texas A&M University, College Station, TX 77807, USA

[3]Department of Molecular and Cell Biology, University of California Berkeley, Berkeley, California 94720, USA.

Keywords: tripartite motif, interferon stimulated genes, TRIM14, TBK1, STAT3, SOCS3, cytosolic DNA sensing, cGAS, innate immunity, IFN, bacterial pathogen, VSV

ABSTRACT

Tripartite motif-containing proteins (TRIMs) play a variety of recently described roles in innate immunity. While many TRIMs regulate type I interferon (IFN) expression following cytosolic nucleic acid sensing of viruses, their contribution to innate immune signaling and gene expression during bacterial infection remains largely unknown. Because *Mycobacterium tuberculosis* is a potent activator of cGAS-dependent cytosolic DNA sensing, we set out to investigate a role for TRIM proteins in regulating macrophage responses to *M. tuberculosis*. Here we demonstrate that TRIM14, a non-canonical TRIM that lacks an E3 ligase RING domain, is a critical negative regulator of the type I IFN response in macrophages. We show that TRIM14 physically interacts with both cGAS and TBK1 and that macrophages lacking TRIM14 dramatically hyperinduce interferon stimulated gene (ISG) expression following cytosolic nucleic acid transfection, IFN-β treatment, and *M. tuberculosis* infection. Consistent with a defect in resolution of the type I IFN response, *Trim14* knockout (KO) macrophages have more phospho-Ser754 STAT3 relative to phospho-727 and fail to upregulate the STAT3 target *Socs3* (Suppressor of Cytokine Signaling 3), which is required to turn off IFNAR signaling. These data support a model whereby TRIM14 acts as a scaffold between TBK1 and STAT3 to promote phosphorylation of STAT3 at Ser727 and enhance negative regulation of ISG expression. Remarkably, *Trim14* KO macrophages hyperinduce antimicrobials like *Inos2* and are significantly better than control cells at limiting *M. tuberculosis* replication. Collectively, these data reveal a previously unappreciated role for TRIM14 in resolving type I IFN responses and controlling *M. tuberculosis* infection.

55 **INTRODUCTION**

56 *Mycobacterium tuberculosis*, arguably the world's most successful pathogen, elicits a
57 carefully orchestrated immune response that allows bacteria to survive and replicate in humans
58 for decades. Infection of macrophages with *M. tuberculosis* sets off a number of pathogen sensing
59 cascades, most notably those downstream of TLR2, which senses mycobacterial lipomannan (1,
60 2), and cGAS, which senses bacterial DNA in the host cytosol (3-5). cGAS-dependent DNA
61 sensing during *M. tuberculosis* infection elicits two distinct and somewhat paradoxical responses:
62 targeting of a population of bacilli for destruction in lysosomes via ubiquitin-mediated selective
63 autophagy, and activation of a type I IFN gene expression program, which is inadequate at
64 controlling bacterial pathogenesis *in vivo*. Because both selective autophagy and type I IFN have
65 been repeatedly shown in animal and human studies to be hugely important in dictating *M.*
66 *tuberculosis* infection outcomes (5-7), there is a critical need to elucidate the molecular
67 mechanisms that drive their activation.

68 Many members of the TRIM family of proteins have emerged as important regulators of a
69 variety of innate immune responses (6-8). Defined on the basis of their tripartite domain
70 architecture, TRIMs generally encode a RING domain with E3 ligase activity, a B-box that is a
71 zinc-binding domain with a RING-like fold (9), and a coil-coiled domain that mediates
72 dimer/multimerization and protein-protein interactions (10). In addition to these domains, TRIMs
73 encode a highly variable C-terminal domain. Since the initial discovery of TRIM5 as a potent HIV
74 restriction factor (11), a variety of TRIMs have been shown to play critical roles in antiviral innate
75 immunity through polyubiquitination of key molecules in DNA and RNA sensing cascades,
76 including MDA5 by TRIM13, TRIM40, and TRIM65 (14-17), RIG-I by TRIM25 and TRIM40 (12,
77 13), and TBK1 by TRIM11 and TRIM23 (14). We are just beginning to appreciate the complex
78 and dynamic network of regulatory factors, including TRIMs, that cells employ to up and
79 downregulate innate immune signaling and gene expression (15).

80 Recent work has shown that cytosolic nucleic acid sensing pathways are also engaged
81 during infection with a variety of intracellular bacterial pathogens, including *M. tuberculosis*,
82 *Legionella pnuemophila*, *Listeria monocytogenes*, *Francisella novicida*, and *Chlamydia*
83 *trachomatis* (16). Some of these pathogens, like *M. tuberculosis and C. trachomatis*, have been
84 shown to activate cGAS via bacterial dsDNA (3, 17), while others like *L. monocytogenes* directly
85 activate STING by secreting cyclic di-AMP (18). It is becoming increasingly clear that activation
86 of cytosolic nucleic acid sensing pathways provides some benefit to intracellular bacterial
87 pathogens, and thus the ability to engage with and manipulate regulatory molecules like TRIM
88 proteins is likely a conserved bacterial adaptation. *Salmonella* Typhimurium has been shown to
89 secrete SopA, an effector molecule which targets TRIM56 and TRIM65 to stimulate innate
90 immune signaling through RIG-I and MDA5 (19, 20). Likewise, TRIM8 has been shown to regulate
91 inflammatory gene expression downstream of TLR3 and TLR4 during *Salmonella* Typhimurium-

92 induced septic shock (21). In addition, ablation of TRIM72 in alveolar macrophages enhances
93 phagocytosis and clearance of *Psuedomonas aeruginosa* (22).
94 Realizing the huge potential for TRIM proteins in tipping the balance between pro- and
95 anti-bacterial innate immune outcomes, we decided to study TRIMs during *M. tuberculosis*
96 infection, specifically a non-canonical TRIM family member: TRIM14. Like most TRIMs, TRIM14
97 encodes a coiled-coil, a B-box, and a C-terminal PRY/SPRY domain, but curiously it lacks the E3
98 ligase RING domain, likely rendering it unable to catalyze ubiquitination of proteins. Consistent
99 with it being a major player in antiviral innate immunity, TRIM14 has been shown to directly
100 influence replication of several RNA viruses including influenza A via interaction with the viral NP
101 protein (23), hepatitis B via interaction with HBx (24), and hepatitis C via interaction with NS5A
102 (25). In the context of RNA sensing, TRIM14 has been shown to localize to mitochondria and
103 interact with the antiviral signaling adapter MAVS (26). More recently, TRIM14 has been shown
104 to promote cGAS stability by recruiting the deubiquitinase USP14 and preventing
105 autophagosomal targeting of cGAS (27).
106 Here, we demonstrate that TRIM14 is a crucial negative regulator of *Ifnb* and ISG
107 expression during macrophage infection with *M. tuberculosis*. TRIM14 is recruited to the *M.*
108 *tuberculosis* phagosome and can directly interact with both cGAS and the DNA sensing kinase
109 TBK1. Deletion of *Trim14* leads to dramatic hyperinduction of *Ifnb* and ISGs in response to *M.*
110 *tuberculosis* and other cytosolic nucleic acid agonists. In *Trim14* KO macrophages we observe
111 preferential phosphorylation of the transcription factor STAT3 at Ser754 and lack of association
112 of STAT3 with the chromatin loci of target genes like Socs3, a crucial negative regulator of
113 interferon α/β receptor (IFNAR) signaling. These data argue that TRIM14 acts as a negative
114 regulator of cytosolic DNA sensing through bringing TBK1 and STAT3 together to promote
115 phosphorylation of STAT3 at Ser727. Surprisingly, *Trim14* KO macrophages were remarkably
116 efficient at limiting *M. tuberculosis* replication by virtue of overexpressing inducible nitric oxide
117 synthase. Collectively, this work suggests that TRIM14 is a critical regulatory node of type I IFN
118 induction and resolution in macrophages and highlights a previously unappreciated role for
119 TRIM14 in anti-*M. tuberculosis* innate immunity.
120
121

122 **MATERIALS AND METHODS**

123 Cell Culture

124 RAW 264.7 macrophages, HEK293T, MEF, and LentiX cells were cultured at 37°C with 5% CO_2.
125 Cell culture medium was comprised of High glucose, sodium pyruvate, Dulbecco's modified Eagle
126 medium (Thermo Fisher) with 10% FBS (Sigma Aldrich) 0.5% HEPES (Thermo Fisher).

127

128 Co-immunoprecipitations

129 1.8 x 10^6 HEK293T cells in a 10cm plate were transfected with 1-10 µg of pDEST 3xFlag TRIM14,
130 pDEST HA cGAS, pDEST HA STING, pDEST HA TBK1, pDEST HA IRF3, pDEST Flag STAT3,
131 or pDEST HA TRIM14 using PolyJet In Vitro DNA Transfection Reagent. Cells were harvested in
132 PBS+0.5M EDTA 24 hours post-transfection and pellets were lysed on ice with lysis buffer (50
133 mM Tris HCl pH 7.4, 150 mM NaCl, 1 mM EDTA, 0.075% NP-40) containing protease inhibitor
134 (Pierce A32955). Strep-tactin superflow plus beads (Qiagen) were washed using buffer containing
135 5% 1M Tris at pH 7.4, 3% NaCl, and 0.2% 0.5M EDTA. 1000 µl of the cleared lysate was added
136 to the beads and inverted for 2 hr at 4°C. Beads were then washed 4 times with wash buffer (50
137 mM Tris HCl pH 7.4 150 mM NaCl 0.5M EDTA, 0.05% NP-40) and eluted using 1x Biotin. Whole
138 cell lysate inputs and elutions were boiled in 4x SDS loading buffer with 10% 2-mercapethanol.
139 Proteins were run on SDS-PAGE gels (Bio-Rad) and then transferred to nitrocellulose membrane
140 (GE Healthcare). Membranes were blocked in TBS (Odyssey Blocking buffer Li-COR) for 1 hour
141 and incubated with primary antibody overnight at 4°C. LI-COR secondary was used (IR Dye CW
142 680 goat anti-rabbit, IR Dye CW 680 goat anti-rat 680, IR Dye CW800 goat anti-mouse (LI-COR))
143 and developed with the Odyssey Fc by LI-COR. Immunoprecipitation experiment were also
144 performed as stated above but with Pierce Anti-HA agarose (Thermo 26181). Beads were eluted
145 three times at room temperature for 15 min each using Influenza Hemagglutinin (HA) peptide
146 (Sigma Aldrich I2149).

147

148 Western Blot analysis

149 Protein samples were run on Any kD Mini-PROTEAN TGX precast protein gels (BioRad) and
150 transferred to 0.45 µm nitrocellulose membranes (GE Healthcare). Membranes were incubated
151 in the primary antibody of interest overnight and washed three times with TBS-Tween 20.
152 Membranes were then incubated in secondary antibody for 1 hour and imaged using LI-COR
153 Odyssey FC Imaging System. Primary antibodies used in this study: mouse monoclonal α-FLAG
154 M2 antibody (Sigma-Aldrich, F3165), α-HA high affinity rat monoclonal antibody (Roche; 3F10),
155 α-strep (Genscript A00626), α-phospho-Stat3 (Ser727) (Cell Signaling #9134), α-phospho-Stat3
156 (Ser754) (Cell Signaling #98543), α-Stat3 (124H6) Mouse mAb (Cell Signaling #9139), α-
157 phospho-Stat1 (Tyr701) (58D6) Rabbit mAb #9167, α-TRIM14 G-15 (Santa Cruz sc79761), α-
158 TRIM14 (Aviva ARP34737), and α-mouse monoclonal Beta-Actin (Abcam, #6276). Secondary

159 antibodies used in this study: IR Dye CW 680 goat anti-rabbit, IR Dye CW 680 goat anti-rat 680,
160 IR Dye CW800 goat anti-mouse (LI-COR), Alexfluor-488 anti-rabbit, Alexfluor-597 anti-rat, and
161 Alexafluo-647 anti-mouse secondary antibodies for immunofluorescence (LI-COR).
162
163 Construction of sgRNA/Cas9 LentiCRISPR and viral transduction
164 Guide RNAs targeting the first exon of Trim14 were designed using the Broad online tool
165 (https://portals.broadinstitute.org/gpp/public/analysis-tools/sgrna-design). The top five hits were
166 used to design five guide RNA constructs that were cloned into Lenti CRISPR vector (Puromycin)
167 at the BsmB1 site. Constructs were sequenced and verified. Plasmids were then transfected into
168 Lenti-X cells with PAX2 and VSVG packing plasmids. Virus was collected 24- and 48-hours post-
169 transfection and stored at -80°C. RAW264.7 cells stably expressing Cas9 were then transduced
170 with virus and selected using puromycin for 72 hours. Cells were then clonally selected using
171 serial dilutions and clones were selected from wells calculated to contain a single cell. To verify
172 the knockout, genomic DNA was collected from cells and the first exon of TRIM14 was amplified
173 using PCR. This reaction was sent for sequencing to verify the mutation.
174
175 Generation of shRNA-expressing stable cell lines
176 To generate knockdown RAW 264.7 macrophages, plasmids of scramble non-targeting shRNA
177 constructs and TRIM14 shRNA constructs targeted towards the 3' UTR of TRIM14 were
178 transfected into Lenti-X cells with PAX2 and VSVG packing plasmids. Virus was collected 24 and
179 48-hours post-transfection and stored at -80°C. RAW264.7 cells were then transduced with virus
180 and selected using hygromycin at 10mg/ml (Invitrogen) to select for cells containing the shRNA
181 plasmid.
182
183 Macrophage stimulation
184 RAW 264.7, CRISPR/Cas9 RAW 264.7, or shRNA RAW 264.7 macrophages were plated on 12-
185 well tissue-culture treated plates at a density of 3×10^5 cells/well and allowed to grow overnight.
186 Cells were then transfected with 1 µg/ml ISD or 1 µg/ml poly(I:C) with lipofectamine or treated
187 with 200units recombinant mouse IFNB (pbl assay science Cat#12400-1).
188
189 *M. tuberculosis* Infection
190 Low passaged lab stocks of each Mtb strain (Erdman strain WT, Erdman *luxBCADE*, or Erdman
191 m-Cherry) were thawed for each experiment to ensure virulence was preserved. *M. tuberculosis*
192 was cultured in roller bottles at 37°C in Middlebrook 7H9 broth (BD Biosciences) supplemented
193 with 10% OADC, 0.5% glycerol, and 0.1% Tween-80. All work with Mtb was performed under
194 Biosafety Level 3 (BSL3) containment using procedures approved by the Texas A&M University
195 Institutional Biosafety Committee. To prepare the inoculum, bacteria grown to log phase (OD 0.6-

196 0.8) were spun at low speed (500g) to remove clumps and then pelleted and washed with PBS
197 twice. Resuspended bacteria were briefly sonicated and spun at low speed once again to further
198 remove clumps. The bacteria were diluted in DMEM + 10% horse serum and added to cells at an
199 MOI of 10 for RNA and cytokine analysis and MOI of 1 for microscopy studies. Cells were spun
200 with bacteria for 10 min at 1000 x g to synchronize infection, washed twice with PBS, and then
201 incubated in fresh media. RAW 264.7 or CRISPR/Cas9 RAW 264.7 macrophages were plated on
202 12-well tissue-culture treated plates at a density of 3×10^5 cells/well and allowed to grow overnight.
203 Where applicable, RNA was harvested from infected cells using 0.5 ml Trizol reagent at each time
204 point.
205
206 *M. tuberculosis* survival/replication
207 RAW 264.7 or CRISPR/Cas9 RAW 264.7 macrophages were plated on 12-well tissue-culture
208 treated plates at a density of 2.5 $x10^5$ cells per well. Luminescence was read for Mtb *luxBCADE*
209 by lysing in 400ul 0.5% Triton-X and splitting into two wells of a 96 well white plate and using the
210 luminescence feature of the INFINITE 200 PRO by TECAN at 0, 24, 48, and 72 hours post
211 infection.
212
213 RNA isolation and qPCR analysis
214 In order to analyze transcripts, cells were harvested in Trizol at the specified time points and RNA
215 was isolated using Direct-zol RNA Miniprep kits (Zymo Research) with 1-hour DNase treatment.
216 cDNA was synthesized with iScript cDNA Synthesis Kit (Bio-Rad). cDNA was diluted to 1:20 for
217 each sample. A pool of cDNA from each treated or infected sample was used to make a 1:10
218 standard curve with each standard sample diluted 1:5 to produce a linear curve. RT-qPCR was
219 performed using Power-Up SYBR Green Master Mix (Thermo Fisher) using a Quant Studio Flex
220 6 (Applied Biosystems). Samples were run in triplicate wells in a 96-well or 384 well plate.
221 Averages of the raw values were normalized to average values for the same sample with the
222 control gene, *beta-actin*. To analyze fold induction, the average of the treated sample was divided
223 by the untreated control sample, which was set at 1.
224
225 Immunofluorescence Microscopy
226 Glass coverslips were incubated in 100μl poly-lysine at 37°C for 30 minutes. MEF cells were
227 plated at a density of $2x10^4$ on glass coverslips in 24-well plates and left to grow overnight. Cells
228 were then transfected with 250ng of the desired plasmid(s) using PolyJet. The next day cells were
229 treated with 1μg ISD as described above. At the designated time points, cells were washed with
230 PBS (Thermo Fisher) and then fixed in 4% paraformaldehyde for 10 minutes. Fixed cells were
231 washed three times in PBS and permeabilized by incubating them in PBS containing 5% non-
232 fat milk and 0.05% saponin (Calbiochem). Coverslips were placed in primary antibody for 1 hour

233 then washed 3x in PBS and placed in secondary antibody. These were washed twice in PBS and
234 twice in deionized water, followed by mounting onto a glass slide using ProLong Diamond antifade
235 mountant (Invitrogen). Images were acquired on a Nikon A1-Confocal Microscope. DAPI nuclear
236 staining (Thermo Fisher).
237
238 Co-localization experiments with *M. tuberculosis*
239 RAW 264.7 macrophages were plated on glass coverslips at a density of 3×10^5 cells/well in 24-
240 well plates. Cells were infected with m-Cherry *M. tuberculosis* at an MOI of 1 and fixed and stained
241 as above at the designated time points. Colocalization of α-TRIM14 G-15 (Santa Cruz sc79761),
242 with *M. tuberculosis* was visualized directly by fluorescence microscopy. A series of images were
243 captured and analyzed by counting the number of bacteria that colocalized with the corresponding
244 marker. At least one hundred events were analyzed per coverslip and each condition was
245 performed with triplicate coverslips.
246
247 Protein Expression and Purification
248 The cDNA encoding mouse TRIM14 (residues 247 to 440), mouse IRF-3 (residues 184-419) were
249 cloned into a modified pET28(a) vector containing an N-terminal Avi-His6-SUMO tag. Sequences
250 of the plasmids were confirmed by DNA sequencing. The BL21 (DE3) cells were co-transformed
251 with the pET28(a) plasmids coding for the target proteins and the pBirAcm plasmid coding for
252 BirA and induced with 0.4 mM IPTG in the presence of 5 μg ml−1 biotin and cultured at 16 °C
253 overnight. The Biotin-labelled-Avi-His6-SUMO proteins were purified using a nickel-NTA column
254 followed by gel-filtration chromatography using a HiLoad 16/60 Superdex 75 column (GE
255 Healthcare). Mouse and human TBK1 (residues 1 to 657) were cloned into the pAcGHLTc
256 baculovirus transfer vector. The plasmid was transfected together with Baculo-Gold bright
257 linearized baculovirus DNA (BD Biosciences) into sf9 insect cells to generate recombinant
258 baculovirus. The original recombinant viruses were amplified for at least two rounds before the
259 large-scale protein expression. The insect cells at a density of 2.5×10^6 cells/ml were infected by
260 TBK1 recombinant baculovirus and cultured at 27°C and harvested 72 hours post infection. The
261 cells were lysed in the buffer containing 150 mM NaCl, 0.2 M Tris-HCl, 1% NP-40, 1 mM PMSF
262 at pH 8.0. The target protein in the supernatant was purified using nickel affinity chromatography
263 followed by size-exclusion chromatography.
264
265 SPR Binding Study
266 The binding studies between mouse TRIM14 and TBK1 were performed using a Biacore X100
267 SPR instrument (GE Healthcare). Biotin-labeled SUMO-fusion TRIM14 was coupled on the
268 sensor chip SA (GE Healthcare). Dilution series of TBK1 or IRF-3 (1.25, 2.5, 5, 10, 20 μM) in 1×
269 HBS-EP+ buffer (GE Healthcare) were injected over the sensor chip at a flow rate of 30 μL/min.

270 The single-cycle kinetic/affinity protocol was used in all binding studies. All measurements were
271 duplicated under the same conditions. The equilibrium K_d was determined by fitting the data to a
272 steady-state 1:1 binding model using Biacore X100 Evaluation software version 2.0 (GE
273 Healthcare).
274
275 Chromatin Immunoprecipitation
276 Chromatin Immunoprecipitation (ChIP) was adapted from Abcam's protocol. Briefly, one confluent
277 15 cm dish of CRISPR/Cas9 RAW 264.7 macrophages were crosslinked in formaldehyde to a
278 final concentration of 0.75% and rotated for 10 minutes. Glycine was added to stop the cross
279 linking by shaking for 5 minutes at a concentration of 125 mM. Cells were rinsed with PBS twice
280 and then scraped into 5 mL PBS and centrifuged at 1,000g for 5 min at 4C. Cellular pellets were
281 resuspended in ChIP lysis buffer (50 mM HEPES-KOH pH7.5, 140 mM NaCl, 1 mM EDTA pH8,
282 1% Triton X-100, 0.1% Sodium Deoxycholate, 0.1% SDS
283 Protease Inhibitors) (750 µL per 1×10^7 cells) and incubated for 10 min on ice. Cellular lysates
284 were sonicated for 40 minutes (30sec ON, 30sec OFF) on high in a Bioruptor UCD-200
285 (Diagenode). After sonication, cellular debris was pelleted by centrifugation for 10 min, 4°C, 8,000
286 × g. Input samples were taken at this step and stored at −80°C until decrosslinking. Approximately
287 25 µg of DNA diluted to 1:10 with RIPA buffer was used for overnight immunoprecipitation. Each
288 ChIP had one sample for the specific antibody and one sample for Protein G beads only which
289 were pre-blocked for 1 hr with single stranded herring sperm DNA (75 ng/µL) and BSA (0.1 µg/µL).
290 The respective primary antibody was added to all samples except the beads-only sample at a
291 concentration of 5 ug and rotated at 4°C overnight. Beads were washed 3x in with a final wash in
292 high salt (500mM NaCl). DNA was eluted with elution buffer and rotated for 15 min at 30C.
293 Centrifuge for 1 min at 2,000 × g and transfer the supernatant into a fresh tube. Supernatant was
294 incubated in NaCl, RNase A (10 mg/mL) and proteinase K (20 mg/mL) and incubated at 65°C for
295 1 h. DNA was purified using phenol:chloroform extraction. DNA levels were measure by RT-
296 qPCR. Primers were designed by tiling each respective gene every 500 base pairs that were
297 inputted into NCBI primer design.
298
299 mRNA sequencing
300 RNA was sequenced from 4 biological replicates for each condition; Uninfected BMDMs, ESX-1-
301 infected BMDMs, and M. tuberculosis-infected BMDMs. Raw reads were processed with expHTS
302 (Street et al. 2015) to trim low-quality sequences and adapter contamination, and to remove PCR
303 duplicates. Trimmed reads for each sample were aligned to the GRCm38 GENCODE primary
304 genome assembly using STAR v.2.5.2b aligner (Dobin et al. 2013), and the GENCODE v.M10
305 annotation (gtf file). Each of the 4 replicates were merged into a single BAM file for further
306 analysis. Prior to analysis, genes with expression less than 2 counts per million reads were

307 filtered, leaving 11,808 genes. Differential gene expression was conducted using a single factor
308 ANOVA model in the limma-voom Bioconductor pipeline. Log2 fold change values with a p-value
309 <0.05 are represented in heatmaps where uninfected samples were the denominator and ESX-1
310 or *M.tuberculosis*-infected samples were the numerator in their respective datasets. Heatmaps
311 were generated with GraphPad Prism Software.
312 VSV infection
313 RAW 264.7 cells were seeded in 12-well plates at $8x10^5$ 16h before infection. Cells were infected
314 with VSV-GFP virus at multiplicity of infection (MOI) of 1 in serum-free DMEM (HyClone
315 SH30022.01). After 1h of incubation with media containing virus, supernatant was removed, and
316 fresh DMEM plus 10% FBS was added to each well. At indicated times post infection, cells were
317 harvested with Trizol and prepared for RNA isolation.
318
319 Statistics
320 Statistical analysis of data was performed using GraphPad Prism software (GraphPad). Two-
321 tailed unpaired Student's t tests were used for statistical analyses, and unless otherwise noted,
322 all results are representative of at least three independent biological experiments and are reported
323 as the mean ± SD (n = 3 per group).
324
325

326 **RESULTS**

327 **TRIM14 is a player in *M. tuberculosis* infection of macrophages**

328 Having previously described a crucial role for the ESX-1 virulence-associated secretion
329 system in eliciting cGAS-dependent cytosolic DNA sensing and type I IFN expression during *M.*
330 *tuberculosis* infection, we first set out to better define gene expression differences in
331 macrophages infected with a wild-type and a ΔESX-1 strain. Briefly, we infected bone marrow
332 derived macrophages (BMDMs) with wild-type *M. tuberculosis* (Erdman strain) and the
333 Tn5370::Rv3877/EccD1 mutant (ΔESX-1) (28), which lacks a functional ESX-1 secretion system
334 and has previously been shown to be defective in eliciting cGAS-dependent responses (29, 30).
335 We performed RNA-seq at an established key innate immune time point of 4h and an average
336 $\log_2$ fold-change of 4 biological replicates is depicted ($p < 0.05$) (Fig. 1A). Consistent with previous
337 microarray and RNA-seq data (30, 31), we observed dramatic induction of pro-inflammatory
338 cytokines (*Il6*, *Il1b*) and antimicrobial molecules like *Inos2* in macrophages infected with both wild-
339 type and ΔESX-1 *M. tuberculosis* (Fig. 1A), alongside downregulation of several protein-coding
340 genes (*Epha2*, *Gpr34*, *Rtn4rl1*), and noncoding RNAs (Gm13391, Gm15564, Gm24270) (Fig.
341 1B). To identify genes/pathways whose induction requires ESX-1 secretion, we performed
342 Ingenuity Pathway Analysis (Qiagen) and identified "Interferon signaling" and "Activation of IRF
343 by Cytosolic PRRs" as the major pathways enriched for ESX-1 dependent genes (Fig. 1C and
344 S1A-B). This analysis is in agreement with earlier data demonstrating a requirement for ESX-1
345 phagosome permeabilization for activation of type I IFN expression downstream of cGAS-
346 dependent cytosolic DNA sensing (30). We next used RT-qPCR to measure expression of a
347 number of important innate immune transcripts, both in BMDMs to validate our RNA-seq results
348 and in RAW 264.7 murine macrophage-like cells (Fig. 1D and S1C), to justify our use of these
349 genetically tractable cells moving forward. We observed almost identical expression of cytokines
350 (*Ifnb*, *Il1b* (Fig. 1D), *Irf7*, Il6 (Fig. S1C)), and antimicrobial molecules (*Rsad2* (Fig. 1D), *Ifit*, *Isg15*,
351 *Gbp1*, *Gbp5*, *Inos2* (Fig. S1C)) and in both cell types, maximal ISG induction was ESX-1-
352 dependent while expression of NFκB genes was ESX-1-independent. In analyzing lists of ESX-
353 1-dependent upregulated genes, we noticed that several belonged to the TRIM family, consistent
354 with TRIMs being ISGs (Fig. 1E) (32). Because so little is known about how TRIM proteins
355 regulate anti-bacterial immunity, we set out to better understand how TRIMs influence cGAS-
356 dependent innate immune outcomes during *M. tuberculosis* infection.

357 Based on its recent characterization as a regulator of cGAS stability (27), we elected to
358 investigate a role for TRIM14 during *M. tuberculosis* infection. RT-qPCR analysis confirmed that
359 *Trim14* expression was upregulated after *M. tuberculosis* infection of RAW 264.7 cells (Fig. 1F).
360 Transfection of RAW 264.7 cells with dsDNA (ISD) (33) recapitulated this effect (Fig. 1F),
361 suggesting that *Trim14* upregulation during *M. tuberculosis* infection occurs downstream of
362 cytosolic DNA sensing. To further implicate TRIM14 in *M. tuberculosis* infection of macrophages,

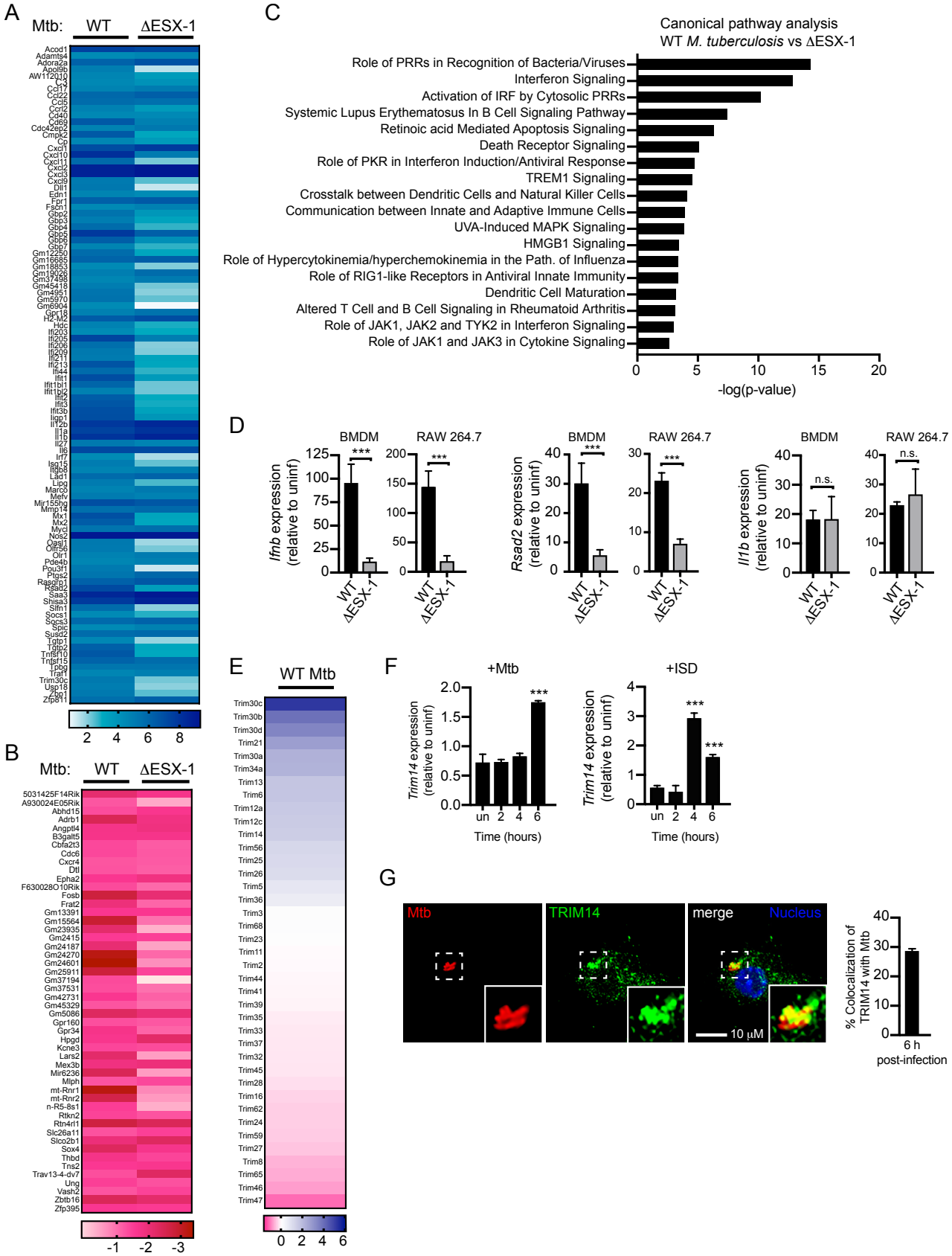

Figure 1: TRIMs are players in the innate immune response to *M. tuberculosis* (A,B) Heatmap of significant ($p < 0.05$) gene expression differences ($\log_2$ fold-change over uninfected) in BMDMs infected with WT vs ΔESX-1 *M. tuberculosis* (Mtb) Genes upregulated are displayed in blue. Genes downregulated are displayed in red. (C) IPA software analysis of cellular pathways enriched for differentially expressed genes in BMDMs infected with WT vs ΔESX-1 *M. tuberculosis*. (D) RT-qPCR of transcripts in BMDMs & RAW 264.7 cells infected with WT *M. tuberculosis*. (E) Heatmap of significant ($p < 0.05$) gene expression differences ($\log_2$ fold-change) in TRIM family genes in BMDMS infected with WT vs ΔESX-1 *M. tuberculosis*. (F) RT-qPCR of fold-change in *Trim14* transcripts in BMDMs stimulated with ISD or infected with WT *M. tuberculosis*, n = 3 biological replicates. (G) RAW 264.7 cells infected with mCherry *M. tuberculosis* for 6 hours and immunostained for TRIM14. Statistical significance was determined using two-tailed students' t test. *$p < 0.05$, **$p < 0.01$, ***$p < 0.001$.

363 we asked whether TRIM14 protein associated with the *M. tuberculosis* phagosome. Using
364 immunofluorescence microscopy and an antibody against endogenous TRIM14, we detected
365 TRIM14 at about 30% of *M. tuberculosis* phagosomes, reminiscent of the number of phagosomes
366 we have previously shown to be positive for ubiquitin (Ub) and LC3, two markers of selective
367 autophagy (Fig. 1G) (34). Together, these data begin to suggest that TRIM14 is a player in the
368 macrophage response to *M. tuberculosis*.
369
370 **TRIM14 interacts with components of the DNA sensing pathway**
371 Based on its recruitment to the *M. tuberculosis* phagosome, we hypothesized that TRIM14
372 may interact with one or more components of the cytosolic DNA sensing pathway (e.g. cGAS,
373 TBK1) that we have previously observed to co-localize with *M. tuberculosis* (Fig. 2A and (3)). We
374 transfected epitope-tagged versions of mouse TRIM14 (3xFLAG-TRIM14) and major components
375 of the DNA sensing pathway (mouse HA-cGAS, HA-STING, and HA-TBK1) into murine embryonic
376 fibroblasts (MEFs). Following 24 hours of expression, cells were fixed, and co-immunostained.
377 Consistent with a previous report (24), we observed that TRIM14 co-localized with cGAS (Fig.
378 2B), while no co-localization between 3xFLAG-TRIM14 and HA-STING was seen. Intriguingly, we
379 also detected substantial overlap between 3xFLAG-TRIM14 and HA-TBK1, suggesting that
380 TRIM14 may interact with more than one component of the cytosolic DNA sensing pathway.
381 To further characterize this previously unappreciated association between TRIM14 and
382 TBK1, we co-expressed mouse 3xFLAG-TRIM14 with mouse HA-cGAS, HA-STING, HA-TBK1,
383 and HA-IRF3 in HEK 293T cells, immunopurified each of the DNA sensing pathway components,
384 and probed for interaction with TRIM14 by western blot. Consistent with our immunofluorescence
385 microscopy data, we found that TRIM14 co-immunoprecipitated with both cGAS and TBK1 but
386 not STING or IRF3 (Fig. 2C).
387 Next, to determine whether these biochemical associations were direct interaction, we
388 performed surface plasmon resonance (SPR) experiments. Briefly, truncated versions of mouse
389 TRIM14 (residues 247-440), human cGAS (residues 157-522), and mouse and human TBK1
390 (residues 11-657) were expressed using a baculovirus system. A portion of mouse IRF3 (residues
391 184-419) served as the negative control (Fig. 2D). Each of these protein truncations had
392 previously been shown to be stably expressed at high levels and remain soluble when generated
393 in insect cells ((35-37) and Fig. S2A). Equilibrium binding studies measured a binding affinity of
394 24.3 μM for binding between mTRIM14 and mTBK1 (Fig. 2E) and a slightly lower affinity of 42.6
395 μM for mouse TRIM14 and a portion of human TBK1 (Fig. 2F). Mouse TRIM14 and full-length
396 hTBK1 also showed direct binding (K_d = 11 μM (Fig. S2D)), as did human cGAS and mouse
397 TRIM14 (K_d = 25.8 μM (Fig. S2B-C)). No binding was measured between mTRIM14 and mIRF3
398 in any of the experiments (Fig. 2E-F and S2C-D). Combined, these *in vivo* and *in vitro* biochemical
399 data argue strongly for a direct interaction between TRIM14 and TBK1.

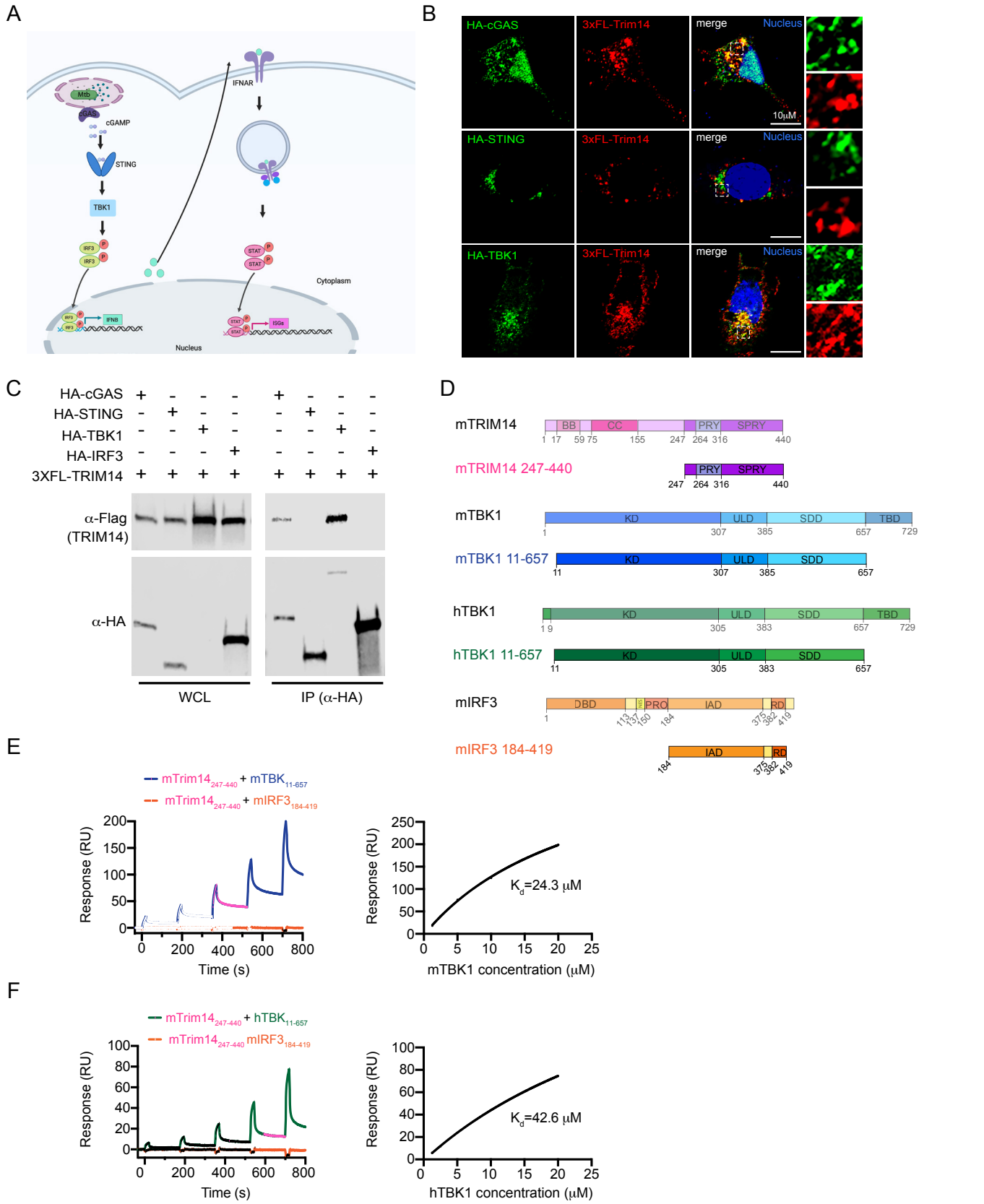

Figure 2: TRIM14 interacts with both cGAS and TBK1 in the DNA sensing pathway (A) Model of DNA sensing pathway during *M. tuberculosis* infection (B) Immunofluorescence microscopy of MEFs expressing 3xFLAG-TRIM14 with HA-cGAS , HA-STING , or HA-TBK1 co-stained with α-HA and α-Flag antibodies (C) Western blot analysis of co-immunoprecipitation of 3xFLAG-TRIM14 co-expressed with HA-cGAS , HA-STING , HA-TBK1, or HA-IRF3 in HEK 293T cells. Blot is representative of >3 independent biological replicates. (D) Diagram of mTRIM14, mTBK1, hTBK1, mIRF3 gene domains and truncations used in surface plasmon resonance (SPR) studies. (E) Equilibrium binding study of mTRIM14 and mTBK1 by SPR. mIRF3 was used as a negative control. Dissociation constant (K_d= 24.3μM) was derived by fitting of the equilibrium binding data to a one-site binding model. (F) As in (E) but with mTRIM14 and hTBK1. Dissociation constant (K_d= 42.6μM) was derived by fitting of the equilibrium binding data to a one-site binding model.

400

401 **Loss of TRIM14 leads to type I IFN and ISG hyperinduction during *M. tuberculosis* infection**

402 To investigate the contribution of TRIM14 to cytosolic DNA sensing outcomes during *M.*
403 *tuberculosis* infection, we first tested how knockdown of *Trim14* affects *Ifnb* gene expression.
404 *Trim14* knockdown (KD) macrophages were generated by transducing RAW 264.7 cells with
405 lentiviral shRNA constructs designed to target the 3'UTR of *Trim14* or a control scramble shRNA
406 (SCR). RT-qPCR analysis confirmed ~50% and 70% knockdown of *Trim14* using two different
407 shRNA constructs (KD1 and KD2 respectively) (Fig. 3A). *Trim14* KD and control RAW 264.7 cells
408 were either infected with *M. tuberculosis* or transfected with ISD to directly engage cGAS and *Ifnb*
409 transcripts were measured after 4 hours. In both experiments, we observed lower levels of *Ifnb*
410 transcript induction in *Trim14* KD cell lines compared to the SCR control (Fig. 3B and 3C),
411 supporting a role for TRIM14 in the DNA sensing pathway. Since residual levels of TRIM14 protein
412 in knockdown cell lines could potentially complicate interpretation of phenotypes, we decided to
413 generate *Trim14* knockouts (KO) using CRISPR-Cas9. Briefly, *Trim14*-specific guide RNAs
414 (gRNAs) were designed to target *Trim14* exon 1 and a GFP-specific gRNA was designed as a
415 negative control. Two clones with distinct frameshift mutations that each introduced a stop codon
416 early in exon 1 were identified and chosen for subsequent experimentation (Fig. 3D). Knockout
417 of *Trim14* was confirmed by western blot using an antibody against the endogenous protein and
418 by anti-TRIM14 immunofluorescence of control and *Trim14* KO cells (Fig. 3E).

419 In order to test how genetic ablation of *Trim14* affects cytosolic DNA sensing, *Trim14* KO
420 and control macrophages were infected with wild type *M. tuberculosis* and RNA was collected
421 over a 24h time-course of infection. Surprisingly, while we again measured lower *Ifnb* expression
422 at 4h post-infection, we observed a dramatic hyperinduction of *Ifnb* in the absence of TRIM14 at
423 later infection time points (Fig. 3F). To determine the contribution of cytosolic DNA sensing to this
424 phenotype, we transfected *Trim14* KO and control RAW 264.7 cells with ISD and again found
425 significantly higher induction of *Ifnb* in the absence of TRIM14 at 8 hours and 24 hours post-
426 transfection (Fig. 3G). To verify that the transcript changes we observed translated to differences
427 in protein levels, we used Interferon Stimulated Response Element (ISRE) luciferase reporter
428 cells to analyze IFN-β protein secretion in supernatants from cells 8- and 24-hours post-*M.*
429 *tuberculosis* infection. Using relative light units as a proxy for IFN-β, we again observed higher
430 production of IFN-β in the absence of TRIM14 (Fig. 3H). These data suggest that the major
431 phenotype associated with *Trim14* ablation in RAW 264.7 macrophages is loss of negative
432 regulation following cytosolic DNA sensing.

433 Having observed higher *Ifnb* transcript and protein levels in *Trim14* KO RAW 264.7 cells,
434 we predicted that these cells would also hyperinduce ISGs following treatment with innate immune
435 agonists that stimulate IRF3 signaling downstream of cGAS or STAT signaling downstream of
436 IFNAR. RT-qPCR analysis of RNA recovered over a time-course of either *M. tuberculosis*

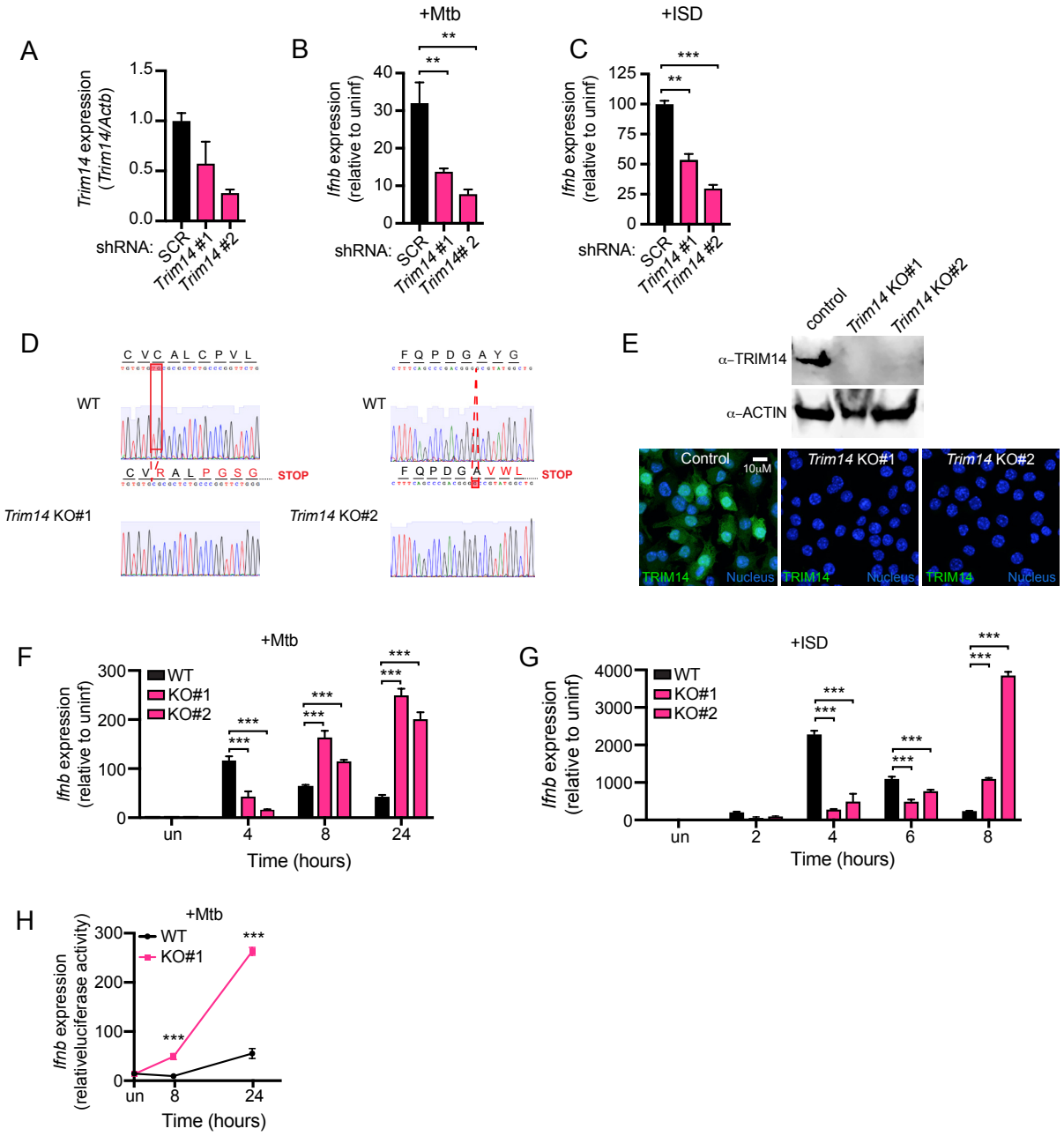

Figure 3: Loss of Trim14 leads to hyperinduction of *Ifnb* in response to *M. tuberculosis* and cytosolic DNA (A) RT-qPCR of *Trim14* transcript in RAW 264.7 macrophages stably expressing shRNA to either SCR control or *Trim14*. (B) RT-qPCR of *Ifnb* transcript in RAW 264.7 macrophages stably expressing shRNA to either SCR control or *Trim14* infected with *M. tuberculosis* at 4h post infection. (C) RT-qPCR of *Ifnb* transcript in RAW 264.7 macrophages stably expressing shRNA to either SCR control or TRIM14 transfected with 1μg ISD at 4h post infection. (D) Sequencing chromatogram depicting mutations in *Trim14* gRNA CRISPR/Cas9 RAW 264.7 macrophages compared to GFP gRNA control (WT). (E) Western blot analysis and immunofluorescence microscopy of *Trim14* in WT vs *Trim14* KO RAW 264.7 macrophages using an anti-TRIM14 antibody. (F) RT-qPCR of *Ifnb* transcripts in WT and *Trim14* KO RAW 264.7 macrophages infected with *M. tuberculosis* at specified times after infection. (G) RT-qPCR of *Ifnb* transcripts in WT and *Trim14* KO RAW 264.7 macrophages treated with ISD at specified times after treatment. (H) ISRE reporter cells expressing luciferase with relative light units measured as a readout for IFN-β protein. All RT-qPCRs represent n = 3 biological replicates. Statistical significance was determined using two-tailed students' t test. *p < 0.05, **p < 0.01, ***p < 0.001.

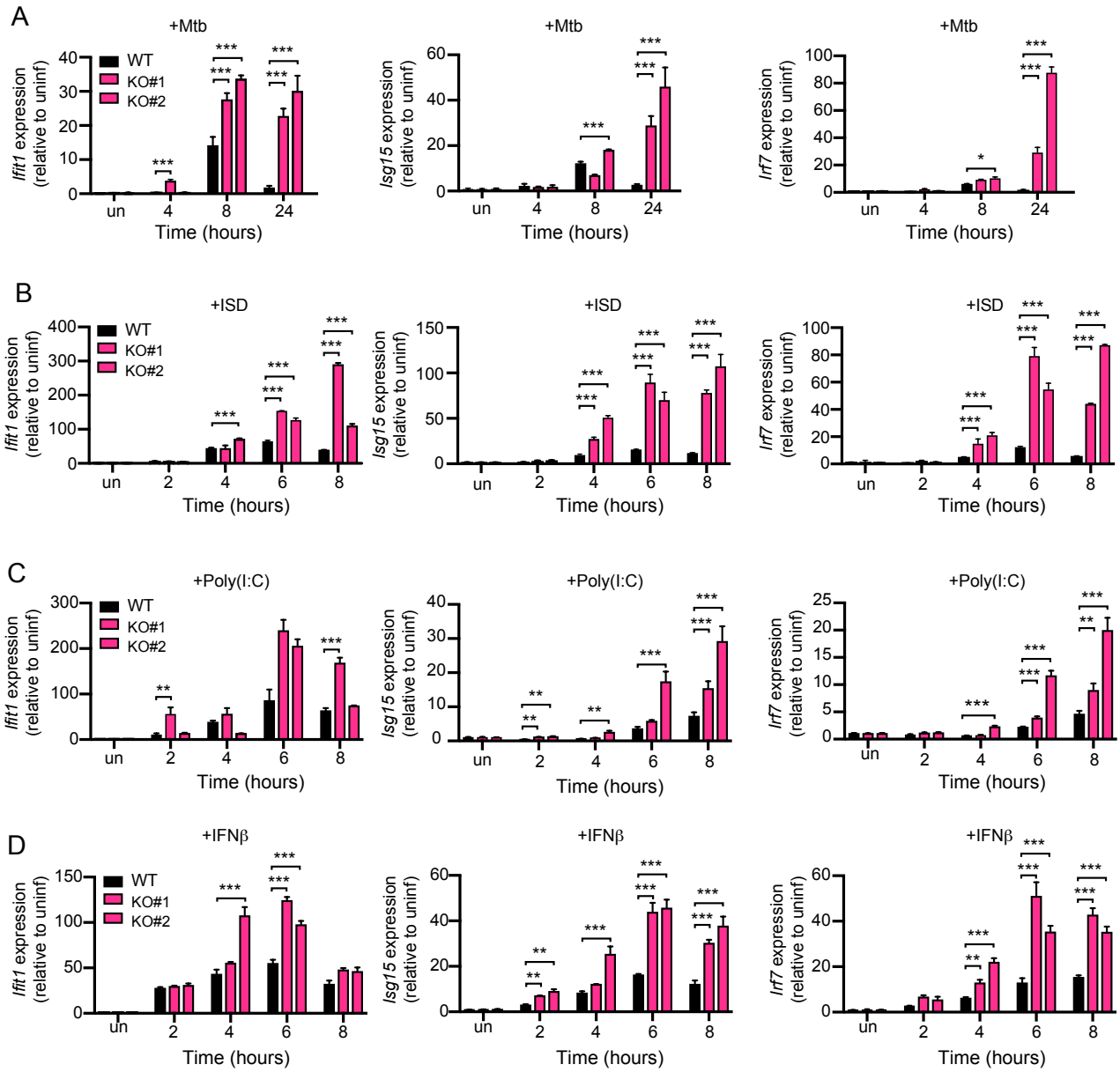

Figure 4: Loss of TRIM14 leads to hyperinduction of ISGs in response to multiple innate immune agonists (A) RT-qPCR of *Ifit*, *Isg15*, *Irf7* transcripts in WT and *Trim14* KO RAW 264.7 macrophages infected with *M. tuberculosis* at specified times after infection. (B) RT-qPCR of *Ifit*, *Isg15*, *Irf7* transcripts in WT and *Trim14* KO RAW 264.7 macrophages transfected with 1μg ISD. (C) As in (B) but with poly(I:C) transfection. (D) As in (B) but with IFNβ treatment (200 IU). All RT-qPCRs represent n = 3 biological replicates. Statistical significance was determined using two-tailed students' t test. *p < 0.05, **p < 0.01, ***p < 0.001.

437 infection or ISD transfection showed hyper induction of *Ifit1*, *Isg15*, and *Irf7* (Fig. 4A and B).
438 Likewise, high levels of these same ISGs were observed when cells were transfected with 1μg
439 poly (I:C), a potent agonist of RNA sensing via RIG-I (Fig. 4C) or treated with recombinant IFN-β
440 directly (Fig. 4D). Importantly, non-ISGs like *Il1b*, *Tnf*, and *Il6*, despite being dramatically induced
441 during *M. tuberculosis* infection were completely unaffected by loss of TRIM14 (Fig. S3A).
442 Collectively, these results demonstrate that TRIM14 is needed for induction of *Ifnb*/ISGs
443 immediately following cGAS sensing as well as for subsequent resolution of the response, arguing
444 for a model whereby TRIM14 regulates cytosolic DNA sensing at two distinct nodes in the
445 pathway.
446
447 **TRIM14 regulates STAT3 activation through TBK1**
448 Since we detected *in vivo* and *in vitro* interactions between TRIM14 and TBK1, we
449 hypothesized that TRIM14-dependent misregulation of TBK1 activity could drive hyperinduction
450 of *Ifnb* and ISGs. TBK1 is a prolific innate immune serine/threonine kinase with many known
451 targets (38, 39). One such target, STAT3 (Signal transducer and activator of transcription 3) has
452 been repeatedly implicated in negatively regulating type I IFN responses (40, 41). Therefore, we
453 set out to determine whether the presence of TRIM14 and its interaction with TBK1 was required
454 to control STAT3 activity in macrophages.
455 Previous studies have demonstrated that TBK1 can directly phosphorylate STAT3 at
456 Ser727 and Ser754 upon cytosolic DNA sensing (45) (Fig. 5A). Phosphorylation of STAT3 at
457 Ser754 inhibits STAT3's ability to interact with target genes, while phosphorylation of STAT3 at
458 Ser727 promotes STAT3 activity and transcription of STAT3 targets (42). To determine whether
459 TRIM14 influences STAT3 phosphorylation, we transfected control and *Trim14* KO cells with ISD
460 to activate TBK1 and analyzed STAT3 phosphorylation at Ser727 and Ser754 by immunoblot
461 over a time-course. We observed substantially more phospho-Ser754 STAT3 and significantly
462 less phospho-Ser727 STAT3 in the absence of TRIM14 (Fig. 5B; replicate blot in Fig. S4B), while
463 loss of TRIM14 had no effect on JAK tyrosine kinase phosphorylation of STAT1 at Y701. These
464 data suggest a role for TRIM14 in influencing TBK1's preference to phosphorylate particular
465 serine residues in the transactivation domain of STAT3. To further implicate TRIM14 in mediating
466 STAT3 activation by TBK1, we performed cellular fractionation experiments and measured the
467 amount of STAT3 in the nucleus following ISD transfection in *Trim14* KO and control cells by
468 immunoblot. Consistent with reduced activation of STAT3, we observed significantly less STAT3
469 accumulation in the nuclei of *Trim14* KO cells (Fig. 5C). We next predicted that TRIM14 can
470 control TBK1's ability to phosphorylate STAT3 by interacting with both factors and bringing them
471 together in a conformation that promotes phosphorylation at STAT3 S727 while inhibiting
472 phosphorylation at S754. Previous studies have demonstrated that TBK1 and STAT3 can co-
473 immunoprecipitate (42). To "close the loop", we tested whether STAT3 and TRIM14 can interact

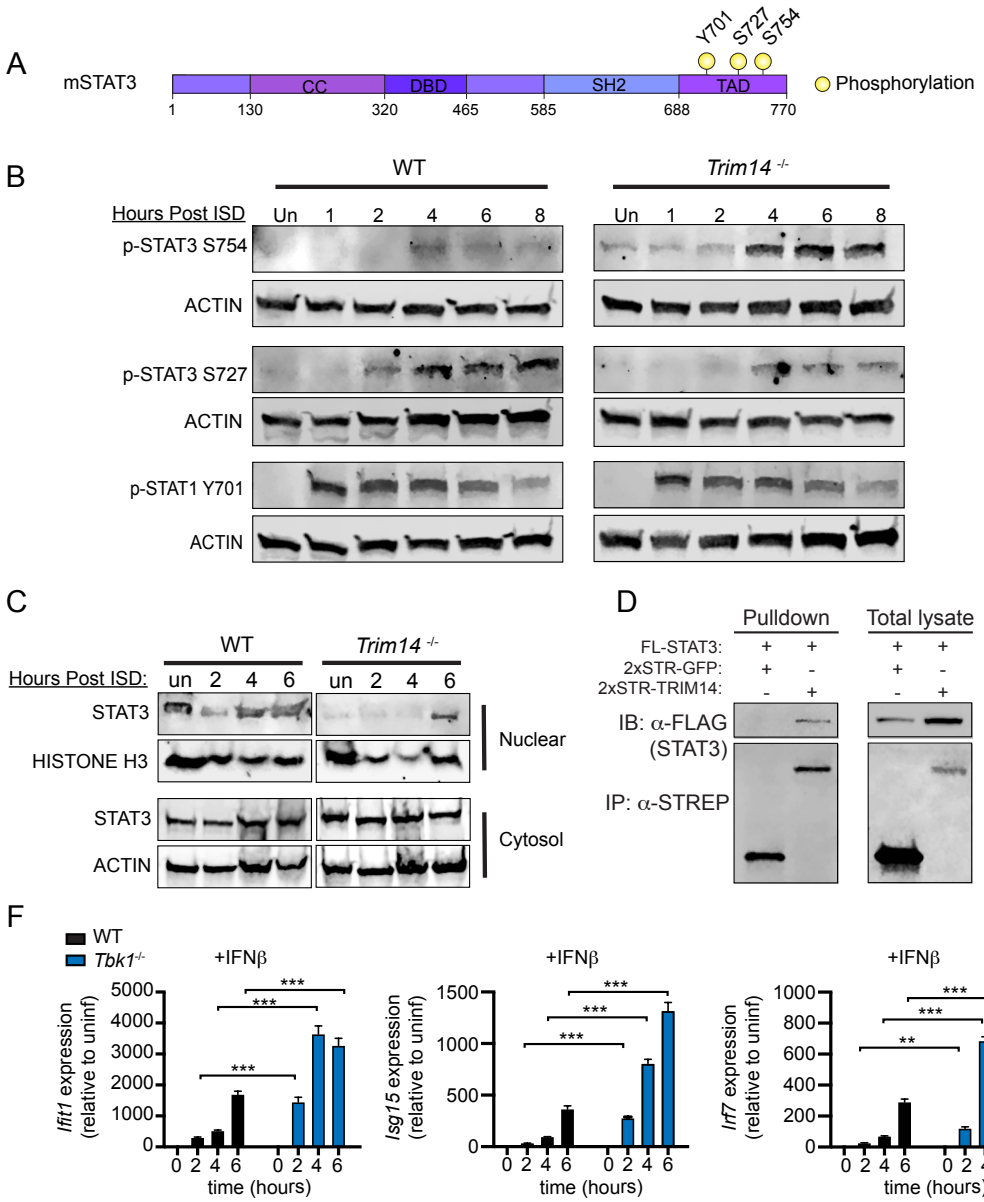

Figure 5: Loss of TRIM14 promotes inhibitory phosphorylation of STAT3 at Ser754 (A) Cartoon depiction of phosphorylation sites of STAT3. (B) Immunoblot of phospho-STAT3 Ser754, phospho-STAT3 Ser727, and phospho-STAT1 Y701 in WT and *Trim14* KO RAW 264.7 macrophages at 1, 2, 4, 6, 8h post-ISD transfection. ACTIN is shown as a loading control. (C) Cellular fractionation showing nuclear STAT3 in WT and *Trim14* KO RAW 264.7 macrophages treated with ISD at specified times after treatment. Histone 3 shown as loading/nuclear control (D) Co-immunoprecipitation and western blot analysis of HEK 293T cells co-transfected with FLAG-STAT3 and HA-TRIM14. (E) RT-qPCR of *Ifit*, *Isg15*, *Irf7* transcripts in WT and *Tbk1* KO BMDMs treated with IFN-β. Western blots are representative of >3 independent biological replicates. Statistical significance was determined using two-tailed students' t test. *p < 0.05, **p < 0.01, ***p < 0.001.

474 when co-expressed in HEK293T cells and indeed, detected association between STAT3 and
475 TRIM14 (Fig. 5D)., We propose that TRIM14, through interactions with STAT3 and TBK1,
476 influences TBK1's ability to phosphorylate STAT3 at particular serine residues.

477 We reasoned that since loss of TRIM14 caused hyperinduction of ISGs via a TBK1/STAT3
478 dependent mechanism, then loss of either TBK1 or STAT3 would phenocopy loss of TRIM14.
479 Indeed, previous studies have shown that *Stat3* KO MEFs and BMDMS hyperinduce ISGs
480 following viral infection (40). To test whether loss of TBK1 could also lead to ISG hyperinduction,
481 we harvested BMDMs from *Tbk1*$^{-/-}$/*Tnfr*$^{-/-}$ mice (43, 44) and treated them with recombinant IFN-β
482 to directly engage with IFNAR and bypass the need for TBK1 to phosphorylate IRF3 and promote
483 *Ifnb* expression (45, 46). Remarkably, we measured dramatic hyperinduction of ISGs in *Tbk1*$^{-/-}$
484 /*Tnfr*$^{-/-}$ BMDMs over a six-hour time course of IFN-β treatment (Fig. 5F). This result argues that
485 TBK1 plays a crucial, yet mostly unappreciated, role in diminishing the type I IFN response
486 downstream of IFNAR signaling and supports a model whereby TRIM14 downregulates type I
487 IFN gene expression via TBK1-dependent phosphorylation of STAT3.
488

489 **TRIM14 is required for STAT3-dependent transcription of *Socs3*, a negative regulator of**
490 **the type I IFN response**

491 Because an uncontrolled type I IFN response is deleterious to the host, cells have evolved
492 multiple mechanisms to dampen type I IFN gene expression following pathogen sensing or IFNAR
493 activation. The hyperinduction of *Ifnb* and ISGs we measure in *Trim14* KO macrophages is
494 consistent with a loss of negative regulation; therefore, we hypothesized that expression of one
495 or more negative regulators would be lower in *Trim14* KO cells. Inhibition of JAK1-STAT signaling
496 is a well-characterized mechanism through which type I IFN signaling is downregulated (47).
497 SOCS (Suppressor of cytokine signaling) family proteins are ISGs that dampen type I IFN
498 responses by interfering with JAK1 kinase activity and limiting STAT signaling (41). USP18
499 (Ubiquitin Specific Peptidase 18) has similarly been shown to inhibit type I IFN expression by
500 blocking interaction between JAK1 and the IFNAR2 subunit (48). To test whether *Trim14* KO cells
501 were defective in expressing negative regulators of the type I IFN response, we measured *Socs3*,
502 *Socs1*, and *Usp18* transcripts in control and *Trim14* KO RAW 264.7 cells infected with *M.*
503 *tuberculosis* or transfected with ISD. Similar to all ISGs we examined in these studies, *Socs1* and
504 *Usp18* were hyperinduced in *Trim14* KO macrophages. However, we observed a specific defect
505 in *Socs3* induction, suggesting that one or more *Socs3* transcription factors were impacted by
506 loss of TRIM14 (Figure 6A and 6B).

507 Previous reports have shown that *Socs3* is a major target gene of STAT3 (49, 50). Having
508 measured increased phosphorylation at the "inhibitory" Ser754 residue of STAT3 in *Trim14* KO
509 macrophages, we hypothesized that lack of *Socs3* induction could be due to the inability of STAT3
510 to bind at the *Socs3* promoter. To test this, we transfected control and *Trim14* KO cells with ISD

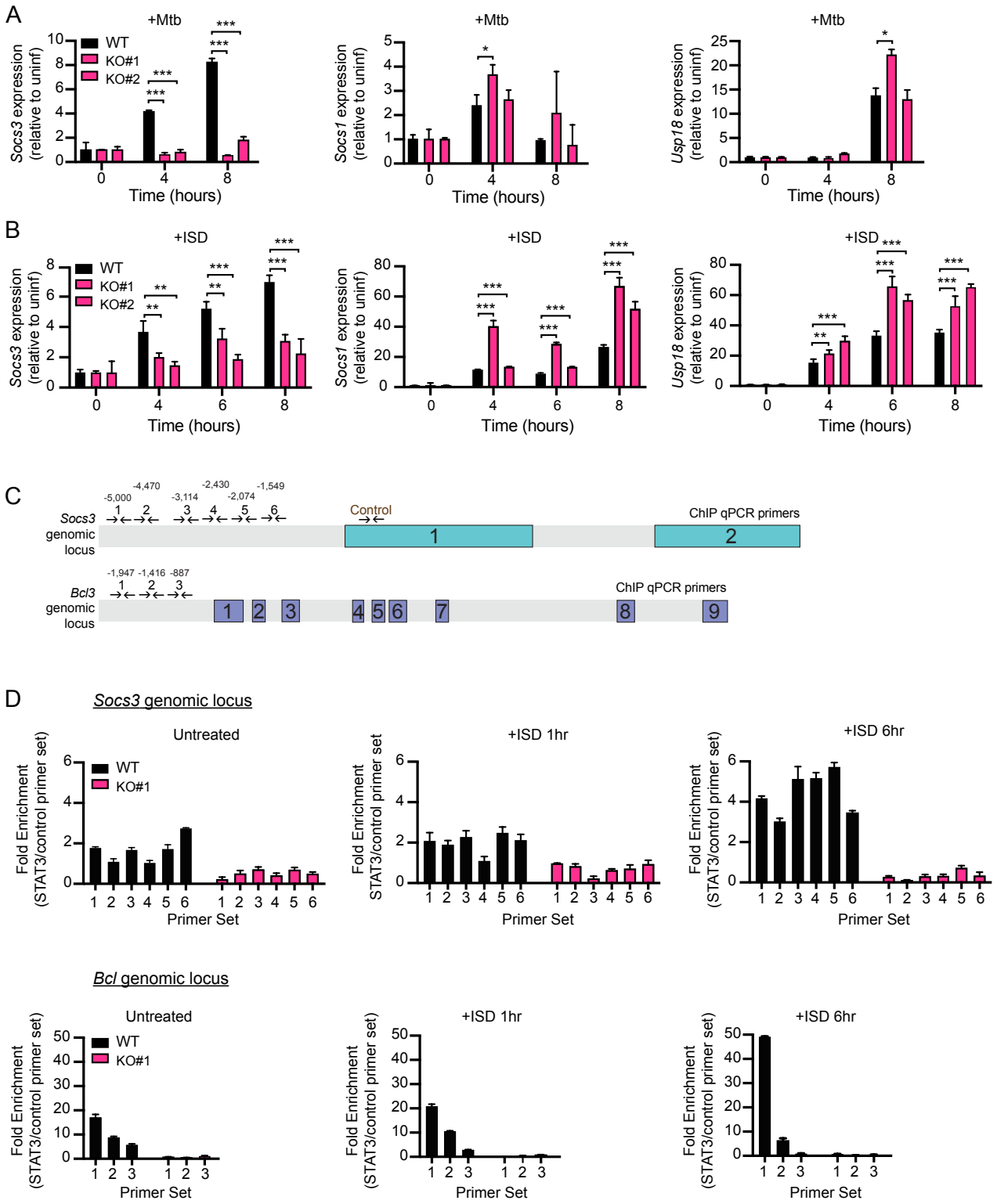

Figure 6: *Trim14* KO macrophages fail to induce expression of the negative regulator of the type I IFN response, Socs3 (A) RT-qPCR of *Socs3*, *Socs1*, and *Usp18* transcripts in WT and *Trim14* KO RAW 264.7 macrophages infected with *M. tuberculosis* at specified times after treatment. (B) RT-qPCR of *Socs3*, *Socs1*, and *Usp18* transcripts in WT and *Trim14* KO RAW 264.7 macrophages treated with ISD at specified times after treatment. (C) qPCR primers designed to tile *Socs3* and *Bcl3* genes for chromatin immunoprecipitation experiments (D) ChIP-qPCR of 3xFLAG-STAT3 associated genomic DNA from the *Socs3* and *Bcl3* loci in WT and *Trim14* KO RAW 264.7 macrophages transfected with 1μg ISD. Statistical significance was determined using two-tailed students' t-test. *p < 0.05, **p < 0.01, ***p < 0.001.

511 and performed chromatin immunoprecipitation (ChIP) at 0h, 1h, and 6h following ISD transfection
512 using an antibody directed against total STAT3 protein. Consistent with low *Socs3* transcription,
513 we detected significantly less recruitment of STAT3 to the *Socs3* genomic locus at both 1h and
514 6h after ISD transfection (Fig. 6D). We also detected lower STAT3 recruitment to other non-ISG
515 target genes, including *Bcl3* (Fig. 6D) and *Cxcl9* (Fig. S3C), suggesting that loss of TRIM14
516 broadly impacts STAT3's ability to translocate to the nucleus and/or associate with DNA. From
517 these data, we conclude that defective nuclear translocation of STAT3 and subsequent lack of
518 *Socs3* transcriptional activation result in ISG hyperinduction in the absence of TRIM14.
519
520 **Loss of TRIM14 impacts the ability of macrophages to control infection**
521 Having demonstrated an important role for TRIM14 in regulating the type I IFN response,
522 we set out to investigate how loss of TRIM14 impacts cell-autonomous innate immune responses
523 to viral and intracellular bacterial infection. To test how loss of TRIM14 impacts survival and
524 replication of *M. tuberculosis*, we infected control and *Trim14* KO macrophages with M.
525 *tuberculosis* expressing the *luxBCADE* operon from *Vibrio harveyi* (51) and quantified bacterial
526 replication as a measure of luminescence over a 72 hour time course (51, 52). Remarkably, we
527 observed a dramatic inhibition of *M. tuberculosis* replication in *Trim14* KO macrophages (Figure
528 7A). Importantly, this lack of *M. tuberculosis* replication did not correspond to loss of cells, as
529 infected monolayers remained completely intact at the 72h time point (Fig. S4A). We also
530 observed a significant inhibition of *M. tuberculosis* replication in *Trim14* KO RAW264.7 cells by
531 enumerating colony forming units (CFUs) (Fig. 7B). To begin to identify the molecular
532 mechanisms driving *M. tuberculosis* restriction in *Trim14* KO macrophages, we measured
533 expression of several genes whose proteins have been purported to have direct bactericidal
534 activity against *M. tuberculosis* (53, 54, 55). RT-qPCR revealed hyperinduction of inducible nitric
535 oxide (*Inos2*) and guanylate binding proteins 1 and 5 (*Gbp1* and *Gbp5*) in *M. tuberculosis*-infected
536 *Trim14* KO macrophages (Fig. 7C). We predict that the overabundance of one or more of these
537 factors contributes to enhanced control of *M. tuberculosis* replication in the absence of TRIM14.
538 Because another report demonstrated that loss of TRIM14 leads to hyperreplication of
539 VSV, an enveloped RNA virus, we also infected TRIM14 KO and control RAW 264.7 cells with
540 VSV and followed viral replication and ISG expression by RT-qPCR over a 12-hour time-course.
541 Although uptake of virus, as inferred by viral genome measurements at the 1h time point was very
542 similar between the two genotypes, we observed a dramatic hyperreplication of VSV in *Trim14*
543 KO macrophages (Fig. S4B) concomitant with significantly higher *Ifnb* and ISG expression (Figure
544 S4D). Although hyperinduction of ISGs is seemingly at odds with hyperreplication of VSV, we do
545 consistently observe low basal levels of *Ifnb* and ISGs in resting macrophages lacking TRIM14
546 (Fig. S4C) (likely due to cGAS instability (27)), which may give the virus enough time to "take off"
547 before TRIM14-dependent resolution of type I IFN responses kicks in.

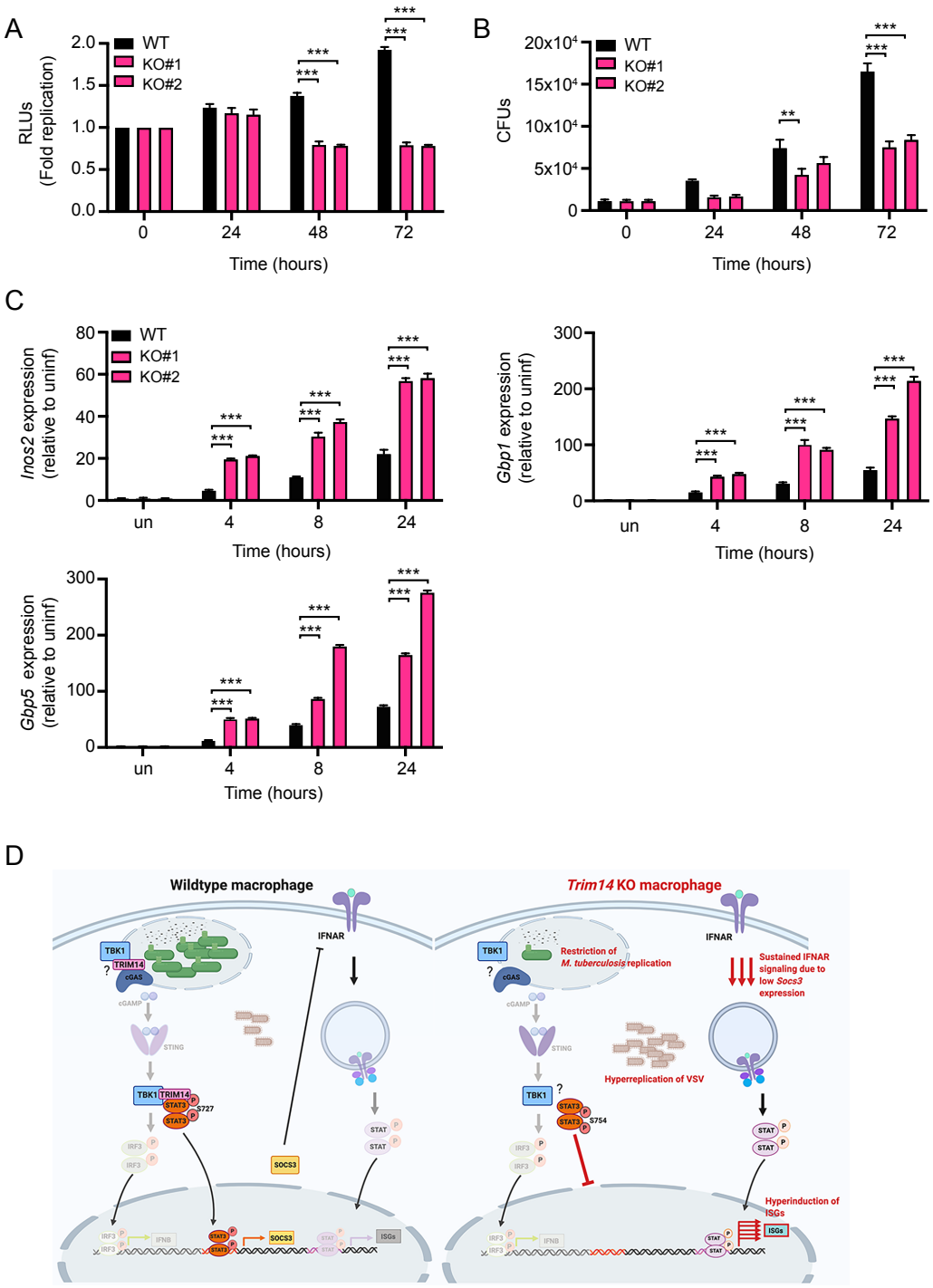

Figure 7: *Trim14* KO macrophages restrict *M. tuberculosis* replication but fail to control VSV replication (A) Fold replication of Mtb *luxBCADE* in WT and *Trim14* KO RAW 264.7 macrophages. (B) CFUs in WT and *Trim14* KO RAW 264.7 macrophages infected with Mtb at 0h, 24h, 48h and 72h post-infection. (C) RT-qPCR of *iNos2, Gbp1*, and *Gbp5* transcript levels in Mtb infected WT and *Trim14* KO RAW 264.7 macrophages. (D) Proposed model of TRIM14's dual roles in regulating cytosolic DNA sensing. TRIM14/cGAS interaction is required to inhibit proteosomal degradation of cGAS and TRIM14/TBK1 interaction is required to promote TBK1-dependent phosphorylation of STAT3 at Ser727 and activate transcription of negative regulators of the type I IFN response like *Socs3*.

548 **DISCUSSION**

549 To prevent chronic inflammation and damage to host cells and tissues, potent innate
550 immune responses like type I IFN induction require tight temporal control. Here, we demonstrate
551 a previously unappreciated role for TRIM14 in resolving *Ifnb* and ISG expression following a
552 variety of cytosolic innate immune stimuli. By providing evidence that TRIM14 can directly interact
553 with both cGAS and TBK1, our work uncovers a complex mechanism through which TRIM14 can
554 both up and downregulate type I IFN responses in macrophages. Notably, we report that loss of
555 TRIM14 has significant consequences on cell autonomous control of both bacterial and viral
556 replication, with dramatic restriction of *M. tuberculosis* replication and uncontrolled replication of
557 VSV observed in *Trim14* KO macrophages (Fig. 7A-B and S4). These results reveal a crucial role
558 for TRIM14 in regulating macrophage innate immunity and point to TRIMs as potential targets for
559 host-directed therapies designed to enhance a macrophage's antimicrobial repertoire.

560 Our data support a model whereby TRIM14 acts as a scaffold between TBK1 and STAT3,
561 promoting TBK1-dependent phosphorylation of STAT3 at Ser727 and transcriptional activation of
562 negative regulators of JAK/STAT signaling like SOCS3 (Figure 7D). There is mounting evidence
563 that a complex network of post-translational modifications regulates STAT3's ability to dimerize,
564 translocate to the nucleus, and/or bind DNA (41). In addition to inhibitory and activating STAT3
565 phosphorylation at Ser754 and Ser727 (42), respectively, several other modifications are known
566 to control STAT3 activity, including acetylation at lysine 685 and phosphorylation of tyrosine 705,
567 both of which increase the protein's ability to bind DNA and translocate to the nucleus (56, 57).
568 We propose that in the context of DNA sensing, TBK1-dependent phosphorylation of STAT3 acts
569 as a control point for ramping up or down the STAT3 transcriptional regulon and the presence of
570 TRIM14 can tip this balance. It is curious that these two modifications (Ser727 and Ser754) have
571 dramatic opposing effects on STAT3 activity, as both residues reside in the transactivation domain
572 in close proximity. Structural studies will be needed to shed light on how modulation of
573 TBK1/STAT3 interactions by TRIM14 promote Ser727 phosphorylation over Ser754
574 phosphorylation. It is possible that the presence of TRIM14 makes one site more accessible either
575 directly through interactions with STAT3 or by modulating interactions with other binding partners
576 that influence availability of one serine over the other.

577 The apparent reliance of *Socs3* on STAT3 for its activation in our RAW 264.7 cells is also
578 notable. In addition to being expressed by STAT3, depending on the cell type and context, *Socs3*
579 can be transcribed by STAT1 and its promoter also contains AP-1, Sp3, and NFκB binding
580 elements (58-60). The fact that these remaining transcription factors do not compensate for loss
581 of STAT3 nuclear translocation in Trim14 KO macrophages (Fig. 5C) hints at the potential for
582 crosstalk between STAT3 and other transcription factors, consistent with previous reports (61-63)
583 and the extent to which the entire STAT3-transcriptional regulon is impacted by loss of TRIM14
584 remains unclear. Furthermore, following STAT3 expression of SOCS3, SOCS3 can actually

585 downregulate STAT3 via a negative feedback loop (64, 65); future experiments will need to
586 determine precisely how this loop is broken in *Trim14* KO macrophages. As STAT3 and SOCS3
587 are hugely important not only for controlling inflammatory responses during infection but also for
588 regulating embryogenesis, cancer metastasis, and apoptosis, there is a critical need to
589 understanding how TRIM14 can regulate their activation (66, 67).

590 Another recent study also shows a requirement for TRIM14 in VSV replication but reported
591 that *Trim14* KO macrophages had lower ISG expression compared to wild-type (27). The authors
592 ascribed these phenotypes to TRIM14's role in promoting cGAS stabilization and provide
593 evidence that loss of TRIM14 allows for cGAS degradation via the E3 ligase USP14 that targets
594 cGAS to p62-dependent selective autophagy. We also observed lower *Ifnb* in response to *M.*
595 *tuberculosis* and ISD transfection for our earliest measurements (4 hours for *M. tuberculosis*
596 infection; 2, 4, and 6 hours for ISD transfection) (Fig. 3B, F, and G), but the phenotype of *Trim14*
597 KO macrophages dramatically shifts to hyperinduction at later time points. It is not entirely clear
598 what accounts for the discrepancies in our data, although notably, our analysis focuses almost
599 exclusively on early time points following viral infection or innate immune activation (1-12 hours)
600 as opposed to the 12-24 hours Chen *et al.* focused on, during which cell death resulting from high
601 viral titers may complicate measurement and interpretation of transcript abundance. Taking the
602 conclusions from both studies into account, it seems likely that TRIM14 plays a dual role in type
603 I IFN regulation whereby it interacts with cGAS to promote type I IFN expression and with
604 TBK1/STAT3 to dampen it (Fig. 7D). Future work will need to investigate the precise
605 spatiotemporal distribution of cGAS/TRIM14-,TBK1/TRIM14-, and STAT3/TRIM14-containing
606 complexes over the course of type I IFN induction and resolution. It will also be important to
607 investigate how and when TRIM14 itself is post-translationally modified. Recent work from Jia *et*
608 *al*., provides evidence for RNF125-mediated polyubiquitination and proteosomal degradation of a
609 mitochondrially-associated population of TRIM14 during viral infection (68). This post-
610 translational modification and others could be critical for controlling whether TRIM14 influences
611 type I IFN responses at the level of cGAS or TBK1/STAT3 or both.

612 Our finding that *Trim14* KO macrophages are better at controlling *M. tuberculosis*
613 replication is quite remarkable. As *M. tuberculosis* replicates very slowly (~24-hour doubling time),
614 we propose that unlike VSV, whose replication can be influenced by low resting ISGs in *Trim14*
615 KO cells, *M. tuberculosis* replication is restricted by hyperinduction of ISGs that dominate after 4
616 hours of infection. It is unlikely that TRIM14's contribution to cGAS stability accounts for *M.*
617 *tuberculosis* restriction in *Trim14* KO macrophages, as our previous work showed that knocking
618 out cGAS actually renders macrophages more permissive to *M. tuberculosis* infection, likely
619 through loss of selective autophagy downstream of cytosolic DNA sensing (3). Consistent with
620 these data and our model, another group has reported that siRNA knockdown of STAT3 in human
621 macrophages enhances nitric oxide synthesis and restricts *M. tuberculosis* replication (69),

622 although it is possible that TRIM14 contributes to *M. tuberculosis* restriction through more direct
623 mechanisms as well. Curiously, in the context of *Listeria monocytogenes* infection of STAT1-
624 deficient fibroblasts, overexpression of TRIM14 was protective, suggesting TRIM14 may have
625 ISG-independent antibacterial functions (70). Future experiments designed to investigate what
626 proteins TRIM14 interacts with on the *M. tuberculosis* phagosome and how loss of TRIM14
627 impacts maturation of the autophagosome will provide important insights into how TRIM14
628 controls *M. tuberculosis* replication and shed light on how we may be able to manipulate TRIM14
629 as a tuberculosis therapeutic.
630
631 **ACKNOWLEDGMENTS**
632 We would like to acknowledge Monica Britton at the University of California, Davis DNA
633 Technologies & Expression Analysis Core Library for her help with initial analysis of our RNA-seq
634 data. We would also like to acknowledge the members of the Patrick and Watson labs for help
635 with editing the manuscript, their valuable discussions, and critical feedback.
636
637

638 **REFERENCES**

639 1. Underhill, D. M., A. Ozinsky, K. D. Smith, and A. Aderem. 1999. Toll-like receptor-2 mediates
640 mycobacteria-induced proinflammatory signaling in macrophages. *Proc. Natl. Acad. Sci. U.S.A.*
641 96: 14459–14463.
642 2. Gilleron, M., J. Nigou, D. Nicolle, V. Quesniaux, and G. Puzo. 2006. The acylation state of
643 mycobacterial lipomannans modulates innate immunity response through toll-like receptor 2.
644 *Chem. Biol.* 13: 39–47.
645 3. Watson, R. O., S. L. Bell, D. A. MacDuff, J. M. Kimmey, E. J. Diner, J. Olivas, R. E. Vance, C.
646 L. Stallings, H. W. Virgin, and J. S. Cox. 2015. The Cytosolic Sensor cGAS Detects
647 Mycobacterium tuberculosis DNA to Induce Type I Interferons and Activate Autophagy. *Cell*
648 *Host Microbe* 17: 811–819.
649 4. Wassermann, R., M. F. Gulen, C. Sala, S. G. Perin, Y. Lou, J. Rybniker, J. L. Schmid-Burgk,
650 T. Schmidt, V. Hornung, S. T. Cole, and A. Ablasser. 2015. Mycobacterium tuberculosis
651 Differentially Activates cGAS- and Inflammasome-Dependent Intracellular Immune Responses
652 through ESX-1. *Cell Host Microbe* 17: 799–810.
653 5. Collins, A. C., H. Cai, T. Li, L. H. Franco, X.-D. Li, V. R. Nair, C. R. Scharn, C. E. Stamm, B.
654 Levine, Z. J. Chen, and M. U. Shiloh. 2015. Cyclic GMP-AMP Synthase Is an Innate Immune
655 DNA Sensor for Mycobacterium tuberculosis. *Cell Host Microbe* 17: 820–828.
656 6. van Gent, M., K. M. J. Sparrer, and M. U. Gack. 2018. TRIM Proteins and Their Roles in
657 Antiviral Host Defenses. *Annu Rev Virol* 5: 385–405.
658 7. Rajsbaum, R., A. García-Sastre, and G. A. Versteeg. 2014. TRIMmunity: the roles of the
659 TRIM E3-ubiquitin ligase family in innate antiviral immunity. *J. Mol. Biol.* 426: 1265–1284.
660 8. Versteeg, G. A., R. Rajsbaum, M. T. Sánchez-Aparicio, A. M. Maestre, J. Valdiviezo, M. Shi,
661 K.-S. Inn, A. Fernandez-Sesma, J. Jung, and A. García-Sastre. 2013. The E3-ligase TRIM
662 family of proteins regulates signaling pathways triggered by innate immune pattern-recognition
663 receptors. *Immunity* 38: 384–398.
664 9. Koliopoulos, M. G., D. Esposito, E. Christodoulou, I. A. Taylor, and K. Rittinger. 2016.
665 Functional role of TRIM E3 ligase oligomerization and regulation of catalytic activity. *EMBO J.*
666 35: 1204–1218.
667 10. Sanchez, J. G., K. Okreglicka, V. Chandrasekaran, J. M. Welker, W. I. Sundquist, and O.
668 Pornillos. 2014. The tripartite motif coiled-coil is an elongated antiparallel hairpin dimer. *Proc.*
669 *Natl. Acad. Sci. U.S.A.* 111: 2494–2499.
670 11. Stremlau, M., C. M. Owens, M. J. Perron, M. Kiessling, P. Autissier, and J. Sodroski. 2004.
671 The cytoplasmic body component TRIM5alpha restricts HIV-1 infection in Old World monkeys.
672 *Nature* 427: 848–853.
673 12. Sanchez, J. G., J. J. Chiang, K. M. J. Sparrer, S. L. Alam, M. Chi, M. D. Roganowicz, B.
674 Sankaran, M. U. Gack, and O. Pornillos. 2016. Mechanism of TRIM25 Catalytic Activation in the
675 Antiviral RIG-I Pathway. *Cell Rep* 16: 1315–1325.
676 13. Zhao, C., M. Jia, H. Song, Z. Yu, W. Wang, Q. Li, L. Zhang, W. Zhao, and X. Cao. 2017.
677 The E3 Ubiquitin Ligase TRIM40 Attenuates Antiviral Immune Responses by Targeting MDA5
678 and RIG-I. *Cell Rep* 21: 1613–1623.
679 14. Sparrer, K. M. J., S. Gableske, M. A. Zurenski, Z. M. Parker, F. Full, G. J. Baumgart, J.
680 Kato, G. Pacheco-Rodriguez, C. Liang, O. Pornillos, J. Moss, M. Vaughan, and M. U. Gack.
681 2017. TRIM23 mediates virus-induced autophagy via activation of TBK1. *Nat Microbiol* 2: 1543–
682 1557.
683 15. Porritt, R. A., and P. J. Hertzog. 2015. Dynamic control of type I IFN signalling by an
684 integrated network of negative regulators. *Trends Immunol.* 36: 150–160.
685 16. Patrick, K. L., S. L. Bell, and R. O. Watson. 2016. For Better or Worse: Cytosolic DNA
686 Sensing during Intracellular Bacterial Infection Induces Potent Innate Immune Responses. *J.*
687 *Mol. Biol.* 428: 3372–3386.
688 17. Zhang, Y., L. Yeruva, A. Marinov, D. Prantner, P. B. Wyrick, V. Lupashin, and U. M.
689 Nagarajan. 2014. The DNA sensor, cyclic GMP-AMP synthase, is essential for induction of IFN-
690 β during Chlamydia trachomatis infection. *J. Immunol.* 193: 2394–2404.
691 18. Woodward, J. J., A. T. Iavarone, and D. A. Portnoy. 2010. c-di-AMP secreted by intracellular
692 Listeria monocytogenes activates a host type I interferon response. *Science* 328: 1703–1705.

693 19. Fiskin, E., S. Bhogaraju, L. Herhaus, S. Kalayil, M. Hahn, and I. Dikic. 2017. Structural basis
694 for the recognition and degradation of host TRIM proteins by Salmonella effector SopA. *Nat*
695 *Commun* 8: 14004–14.
696 20. Kamanova, J., H. Sun, M. Lara-Tejero, and J. E. Galán. 2016. The Salmonella Effector
697 Protein SopA Modulates Innate Immune Responses by Targeting TRIM E3 Ligase Family
698 Members. *PLoS Pathog.* 12: e1005552.
699 21. Ye, W., M.-M. Hu, C.-Q. Lei, Q. Zhou, H. Lin, M.-S. Sun, and H.-B. Shu. 2017. TRIM8
700 Negatively Regulates TLR3/4-Mediated Innate Immune Response by Blocking TRIF-TBK1
701 Interaction. *J. Immunol.* 199: 1856–1864.
702 22. Nagre, N., X. Cong, H.-L. Ji, J. M. Schreiber, H. Fu, I. Pepper, S. Warren, J. M. Sill, R. D.
703 Hubmayr, and X. Zhao. 2018. Inhaled TRIM72 Protein Protects Ventilation Injury to the Lung
704 through Injury-guided Cell Repair. *Am. J. Respir. Cell Mol. Biol.* 59: 635–647.
705 23. Wu, X., J. Wang, S. Wang, F. Wu, Z. Chen, C. Li, G. Cheng, and F. X.-F. Qin. 2019.
706 Inhibition of Influenza A Virus Replication by TRIM14 via Its Multifaceted Protein-Protein
707 Interaction With NP. *Front Microbiol* 10: 344.
708 24. Tan, G., F. Xu, H. Song, Y. Yuan, Q. Xiao, F. Ma, F. X.-F. Qin, and G. Cheng. 2018.
709 Identification of TRIM14 as a Type I IFN-Stimulated Gene Controlling Hepatitis B Virus
710 Replication by Targeting HBx. *Front Immunol* 9: 1872.
711 25. Wang, S., Y. Chen, C. Li, Y. Wu, L. Guo, C. Peng, Y. Huang, G. Cheng, and F. X.-F. Qin.
712 2016. TRIM14 inhibits hepatitis C virus infection by SPRY domain-dependent targeted
713 degradation of the viral NS5A protein. *Sci Rep* 6: 32336–12.
714 26. Zhou, Z., X. Jia, Q. Xue, Z. Dou, Y. Ma, Z. Zhao, Z. Jiang, B. He, Q. Jin, and J. Wang. 2014.
715 TRIM14 is a mitochondrial adaptor that facilitates retinoic acid-inducible gene-I-like receptor-
716 mediated innate immune response. *Proc. Natl. Acad. Sci. U.S.A.* 111: E245–54.
717 27. Chen, M., Q. Meng, Y. Qin, P. Liang, P. Tan, L. He, Y. Zhou, Y. Chen, J. Huang, R.-F.
718 Wang, and J. Cui. 2016. TRIM14 Inhibits cGAS Degradation Mediated by Selective Autophagy
719 Receptor p62 to Promote Innate Immune Responses. *Mol. Cell* 64: 105–119.
720 28. Stanley, S. A., S. Raghavan, W. W. Hwang, and J. S. Cox. 2003. Acute infection and
721 macrophage subversion by Mycobacterium tuberculosis require a specialized secretion system.
722 *Proc. Natl. Acad. Sci. U.S.A.* 100: 13001–13006.
723 29. Stanley, S. A., J. E. Johndrow, P. Manzanillo, and J. S. Cox. 2007. The Type I IFN response
724 to infection with Mycobacterium tuberculosis requires ESX-1-mediated secretion and contributes
725 to pathogenesis. *J. Immunol.* 178: 3143–3152.
726 30. Manzanillo, P. S., M. U. Shiloh, D. A. Portnoy, and J. S. Cox. 2012. Mycobacterium
727 tuberculosis activates the DNA-dependent cytosolic surveillance pathway within macrophages.
728 *Cell Host Microbe* 11: 469–480.
729 31. Andreu, N., J. Phelan, P. F. de Sessions, J. M. Cliff, T. G. Clark, and M. L. Hibberd. 2017.
730 Primary macrophages and J774 cells respond differently to infection with Mycobacterium
731 tuberculosis. *Sci Rep* 7: 42225–12.
732 32. Schoggins, J. W., D. A. MacDuff, N. Imanaka, M. D. Gainey, B. Shrestha, J. L. Eitson, K. B.
733 Mar, R. B. Richardson, A. V. Ratushny, V. Litvak, R. Dabelic, B. Manicassamy, J. D. Aitchison,
734 A. Aderem, R. M. Elliott, A. García-Sastre, V. Racaniello, E. J. Snijder, W. M. Yokoyama, M. S.
735 Diamond, H. W. Virgin, and C. M. Rice. 2014. Pan-viral specificity of IFN-induced genes reveals
736 new roles for cGAS in innate immunity. *Nature* 505: 691–695.
737 33. Stetson, D. B., and R. Medzhitov. 2006. Recognition of cytosolic DNA activates an IRF3-
738 dependent innate immune response. *Immunity* 24: 93–103.
739 34. Watson, R. O., P. S. Manzanillo, and J. S. Cox. 2012. Extracellular M. tuberculosis DNA
740 targets bacteria for autophagy by activating the host DNA-sensing pathway. *Cell* 150: 803–815.
741 35. Li, X., C. Shu, G. Yi, C. T. Chaton, C. L. Shelton, J. Diao, X. Zuo, C. C. Kao, A. B. Herr, and
742 P. Li. 2013. Cyclic GMP-AMP synthase is activated by double-stranded DNA-induced
743 oligomerization. *Immunity* 39: 1019–1031.
744 36. Shu, C., B. Sankaran, C. T. Chaton, A. B. Herr, A. Mishra, J. Peng, and P. Li. 2013.
745 Structural insights into the functions of TBK1 in innate antimicrobial immunity. *Structure* 21:
746 1137–1148.

747 37. Larabi, A., J. M. Devos, S.-L. Ng, M. H. Nanao, A. Round, T. Maniatis, and D. Panne. 2013.
748 Crystal structure and mechanism of activation of TANK-binding kinase 1. *Cell Rep* 3: 734–746.
749 38. Helgason, E., Q. T. Phung, and E. C. Dueber. 2013. Recent insights into the complexity of
750 Tank-binding kinase 1 signaling networks: the emerging role of cellular localization in the
751 activation and substrate specificity of TBK1. *FEBS Lett.* 587: 1230–1237.
752 39. Weidberg, H., and Z. Elazar. 2011. TBK1 mediates crosstalk between the innate immune
753 response and autophagy. *Sci Signal* 4: pe39–pe39.
754 40. Wang, W.-B., D. E. Levy, and C.-K. Lee. 2011. STAT3 negatively regulates type I IFN-
755 mediated antiviral response. *J. Immunol.* 187: 2578–2585.
756 41. Tsai, M.-H., L.-M. Pai, and C.-K. Lee. 2019. Fine-Tuning of Type I Interferon Response by
757 STAT3. *Front Immunol* 10: 1448.
758 42. Hsia, H.-C., J. E. Hutti, and A. S. Baldwin. 2017. Cytosolic DNA Promotes Signal
759 Transducer and Activator of Transcription 3 (STAT3) Phosphorylation by TANK-binding Kinase
760 1 (TBK1) to Restrain STAT3 Activity. *J. Biol. Chem.* 292: 5405–5417.
761 43. Hemmi, H., O. Takeuchi, S. Sato, M. Yamamoto, T. Kaisho, H. Sanjo, T. Kawai, K. Hoshino,
762 K. Takeda, and S. Akira. 2004. The roles of two IkappaB kinase-related kinases in
763 lipopolysaccharide and double stranded RNA signaling and viral infection. *J. Exp. Med.* 199:
764 1641–1650.
765 44. Perry, A. K., E. K. Chow, J. B. Goodnough, W.-C. Yeh, and G. Cheng. 2004. Differential
766 requirement for TANK-binding kinase-1 in type I interferon responses to toll-like receptor
767 activation and viral infection. *J. Exp. Med.* 199: 1651–1658.
768 45. Fitzgerald, K. A., S. M. McWhirter, K. L. Faia, D. C. Rowe, E. Latz, D. T. Golenbock, A. J.
769 Coyle, S.-M. Liao, and T. Maniatis. 2003. IKKepsilon and TBK1 are essential components of the
770 IRF3 signaling pathway. *Nat. Immunol.* 4: 491–496.
771 46. Tanaka, Y., and Z. J. Chen. 2012. STING specifies IRF3 phosphorylation by TBK1 in the
772 cytosolic DNA signaling pathway. *Sci Signal* 5: ra20–ra20.
773 47. Ivashkiv, L. B., and L. T. Donlin. 2014. Regulation of type I interferon responses. *Nat. Rev.*
774 *Immunol.* 14: 36–49.
775 48. Honke, N., N. Shaabani, D.-E. Zhang, C. Hardt, and K. S. Lang. 2016. Multiple functions of
776 USP18. *Cell Death Dis* 7: e2444–e2444.
777 49. Hutchins, A. P., D. Diez, Y. Takahashi, S. Ahmad, R. Jauch, M. L. Tremblay, and D.
778 Miranda-Saavedra. 2013. Distinct transcriptional regulatory modules underlie STAT3's cell type-
779 independent and cell type-specific functions. *Nucleic Acids Res.* 41: 2155–2170.
780 50. Ramadoss, P., N. E. Unger-Smith, F. S. Lam, and A. N. Hollenberg. 2009. STAT3 targets
781 the regulatory regions of gluconeogenic genes in vivo. *Mol. Endocrinol.* 23: 827–837.
782 51. Penn, B. H., Z. Netter, J. R. Johnson, J. von Dollen, G. M. Jang, T. Johnson, Y. M. Ohol, C.
783 Maher, S. L. Bell, K. Geiger, G. Golovkine, X. Du, A. Choi, T. Parry, B. C. Mohapatra, M. D.
784 Storck, H. Band, C. Chen, S. Jäger, M. Shales, D. A. Portnoy, R. Hernandez, L. Coscoy, J. S.
785 Cox, and N. J. Krogan. 2018. An Mtb-Human Protein-Protein Interaction Map Identifies a Switch
786 between Host Antiviral and Antibacterial Responses. *Mol. Cell* 71: 637–648.e5.
787 52. Roberts, A. W., L. M. Popov, G. Mitchell, K. L. Ching, D. J. Licht, G. Golovkine, G. M.
788 Barton, and J. S. Cox. 2019. Cas9+ conditionally-immortalized macrophages as a tool for
789 bacterial pathogenesis and beyond. *Elife* 8: 1287.
790 53. MacMicking, J. D. 2014. Cell-autonomous effector mechanisms against mycobacterium
791 tuberculosis. *Cold Spring Harb Perspect Med* 4: a018507–a018507.
792 54. MacMicking, J. D., R. J. North, R. LaCourse, J. S. Mudgett, S. K. Shah, and C. F. Nathan.
793 1997. Identification of nitric oxide synthase as a protective locus against tuberculosis. *Proc.*
794 *Natl. Acad. Sci. U.S.A.* 94: 5243–5248.
795 55. Kim, B.-H., A. R. Shenoy, P. Kumar, R. Das, S. Tiwari, and J. D. MacMicking. 2011. A family
796 of IFN-γ-inducible 65-kD GTPases protects against bacterial infection. *Science* 332: 717–721.
797 56. Zhuang, S. 2013. Regulation of STAT signaling by acetylation. *Cell. Signal.* 25: 1924–1931.
798 57. Wang, R., P. Cherukuri, and J. Luo. 2005. Activation of Stat3 sequence-specific DNA
799 binding and transcription by p300/CREB-binding protein-mediated acetylation. *J. Biol. Chem.*
800 280: 11528–11534.

801 58. Wiejak, J., J. Dunlop, S. Gao, G. Borland, and S. J. Yarwood. 2012. Extracellular signal-
802 regulated kinase mitogen-activated protein kinase-dependent SOCS-3 gene induction requires
803 c-Jun, signal transducer and activator of transcription 3, and specificity protein 3 transcription
804 factors. *Mol. Pharmacol.* 81: 657–668.
805 59. Yang, J., J. Huang, M. Dasgupta, N. Sears, M. Miyagi, B. Wang, M. R. Chance, X. Chen, Y.
806 Du, Y. Wang, L. An, Q. Wang, T. Lu, X. Zhang, Z. Wang, and G. R. Stark. 2010. Reversible
807 methylation of promoter-bound STAT3 by histone-modifying enzymes. *Proc. Natl. Acad. Sci.*
808 *U.S.A.* 107: 21499–21504.
809 60. Isobe, A., T. Takeda, M. Sakata, T. Yamamoto, R. Minekawa, M. Hayashi, C. J.
810 Auernhammer, K. Tasaka, and Y. Murata. 2006. STAT3-mediated constitutive expression of
811 SOCS3 in an undifferentiated rat trophoblast-like cell line. *Placenta* 27: 912–918.
812 61. Grivennikov, S. I., and M. Karin. 2010. Dangerous liaisons: STAT3 and NF-kappaB
813 collaboration and crosstalk in cancer. *Cytokine Growth Factor Rev.* 21: 11–19.
814 62. Kesanakurti, D., C. Chetty, D. Rajasekhar Maddirela, M. Gujrati, and J. S. Rao. 2013.
815 Essential role of cooperative NF-κB and Stat3 recruitment to ICAM-1 intronic consensus
816 elements in the regulation of radiation-induced invasion and migration in glioma. *Oncogene* 32:
817 5144–5155.
818 63. Yu, Z., and B. C. Kone. 2004. The STAT3 DNA-binding domain mediates interaction with
819 NF-kappaB p65 and inducible nitric oxide synthase transrepression in mesangial cells. *J. Am.*
820 *Soc. Nephrol.* 15: 585–591.
821 64. Huang, L., B. Hu, J. Ni, J. Wu, W. Jiang, C. Chen, L. Yang, Y. Zeng, R. Wan, G. Hu, and X.
822 Wang. 2016. Transcriptional repression of SOCS3 mediated by IL-6/STAT3 signaling via
823 DNMT1 promotes pancreatic cancer growth and metastasis. *J. Exp. Clin. Cancer Res.* 35: 27.
824 65. Lu, Y., S. Fukuyama, R. Yoshida, T. Kobayashi, K. Saeki, H. Shiraishi, A. Yoshimura, and
825 G. Takaesu. 2006. Loss of SOCS3 gene expression converts STAT3 function from anti-
826 apoptotic to pro-apoptotic. *J. Biol. Chem.* 281: 36683–36690.
827 66. Siveen, K. S., S. Sikka, R. Surana, X. Dai, J. Zhang, A. P. Kumar, B. K. H. Tan, G. Sethi,
828 and A. Bishayee. 2014. Targeting the STAT3 signaling pathway in cancer: role of synthetic and
829 natural inhibitors. *Biochim. Biophys. Acta* 1845: 136–154.
830 67. Resemann, H. K., C. J. Watson, and B. Lloyd-Lewis. 2014. The Stat3 paradox: a killer and
831 an oncogene. *Mol. Cell. Endocrinol.* 382: 603–611.
832 68. Jia, X., H. Zhou, C. Wu, Q. Wu, S. Ma, C. Wei, Y. Cao, J. Song, H. Zhong, Z. Zhou, and J.
833 Wang. 2017. The Ubiquitin Ligase RNF125 Targets Innate Immune Adaptor Protein TRIM14 for
834 Ubiquitination and Degradation. *J. Immunol.* 198: 4652–4658.
835 69. Queval, C. J., O.-R. Song, N. Deboosère, V. Delorme, A.-S. Debrie, R. Iantomasi, R.
836 Veyron-Churlet, S. Jouny, K. Redhage, G. Deloison, A. Baulard, M. Chamaillard, C. Locht, and
837 P. Brodin. 2016. STAT3 Represses Nitric Oxide Synthesis in Human Macrophages upon
838 Mycobacterium tuberculosis Infection. *Sci Rep* 6: 29297.
839 70. Perelman, S. S., M. E. Abrams, J. L. Eitson, D. Chen, A. Jimenez, M. Mettlen, J. W.
840 Schoggins, and N. M. Alto. 2016. Cell-Based Screen Identifies Human Interferon-Stimulated
841 Regulators of Listeria monocytogenes Infection. *PLoS Pathog.* 12: e1006102.
842

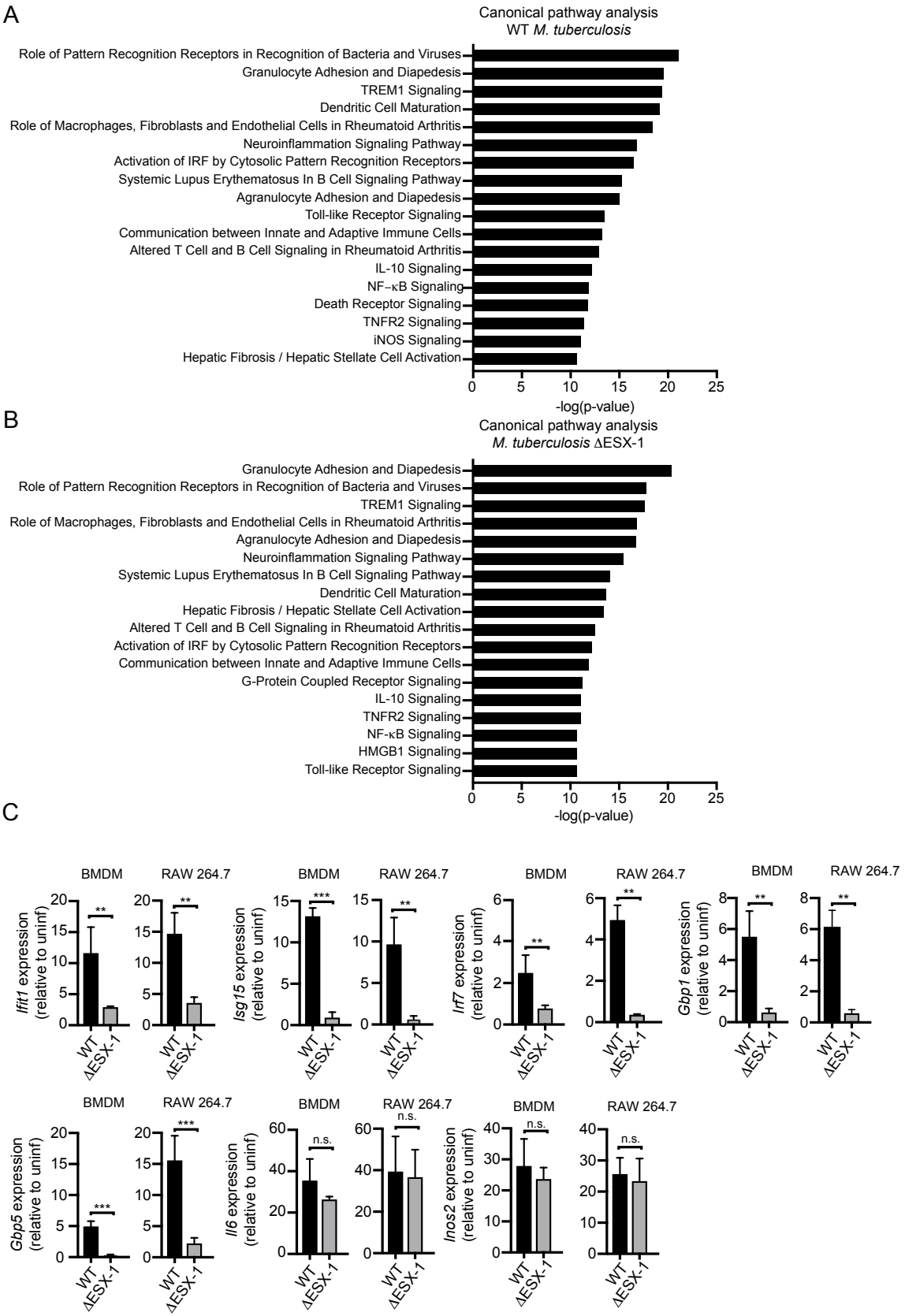

Figure S1. (A) IPA software analysis of cellular pathways enriched for differentially expressed genes in BMDMs infected with WT *M. tuberculosis*. (B) IPA software analysis of cellular pathways enriched for differentially expressed genes in BMDMs infected with ΔESX-1 *M. tuberculosis*. (C) RT-qPCR of transcripts in BMDMs & RAW 264.7 cells infected with WT *M. tuberculosis.*

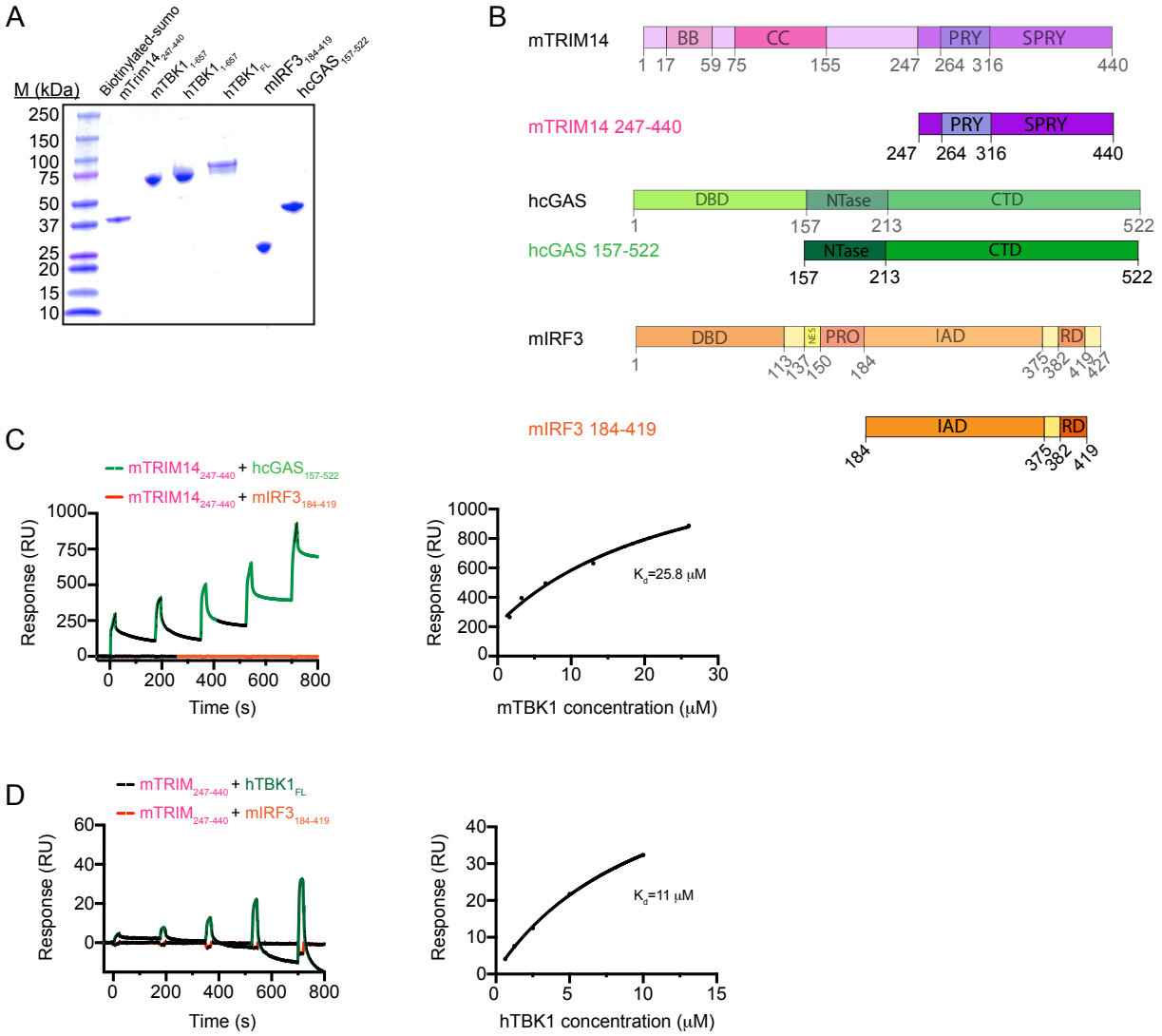

Figure S2. (A) Protein expression of mTRIM14, mTBK1, hTBK1, mIRF3, and hcGAS. (B) Diagram of mTRIM14, mIRF3, and hcGAS gene domains and truncations used in SPR studies. (C) Equilibrium binding study of mTRIM14 and hcGAS by surface plasmon resonance (SPR). mIRF3 was used as a negative control. Dissociation constant (K_d= 25.8 μM) was derived by fitting of the equilibrium binding data to a one-site binding model. Equilibrium binding study of mTRIM14 and hTBK1 by surface plasmon resonance (SPR). mIRF3 was used as a negative control. Dissociation constant (K_d= 11 μM) was derived by fitting of the equilibrium binding data to a one-site binding model.

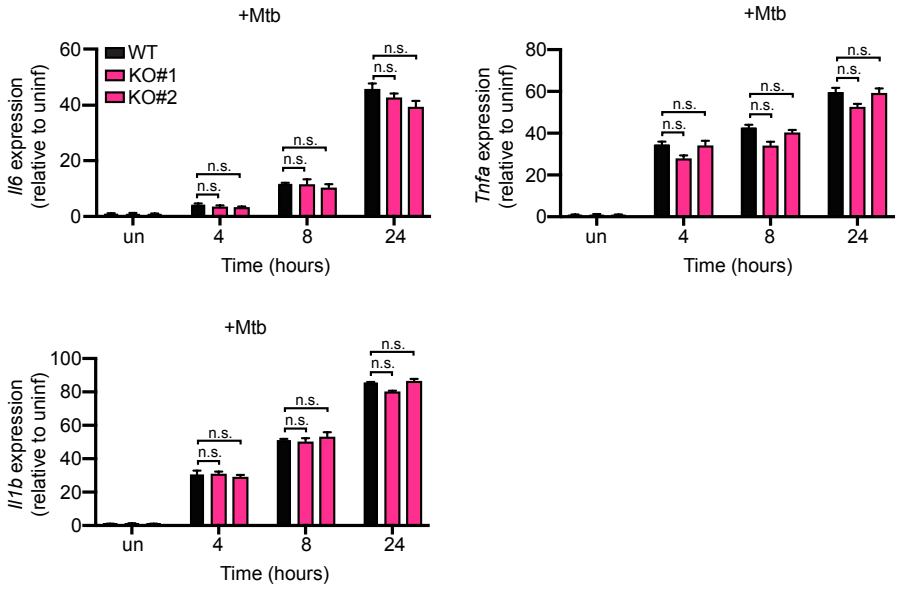

Figure S3. (A) RT-qPCR of *Il6, Tnfa,* and *Il1b* transcripts in WT and *Trim14* KO RAW 264.7 macrophages infected with *M. tuberculosis* at specified times after infection.

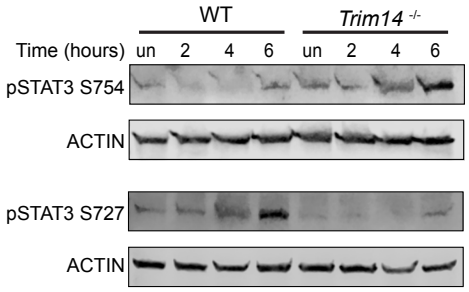

Figure S4. Immunoblot of phospho-STAT3 Ser754, phospho-STAT3 Ser727, and phospho-STAT1 Y701 in WT and *Trim14* KO RAW 264.7 macrophages at 1, 2, 4, 6, 8h post recombinant IFNb treatment. ACTIN is shown as a loading control.

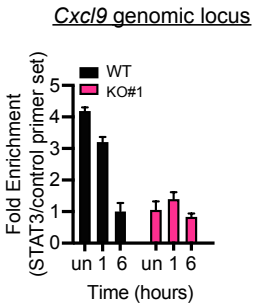

Figure S5. ChIP-qPCR of 3xFLAG-STAT3 associated genomic DNA from the CXCL9 locus in WT and *Trim14* KO RAW 264.7 macrophages transfected with 1 μg ISD.

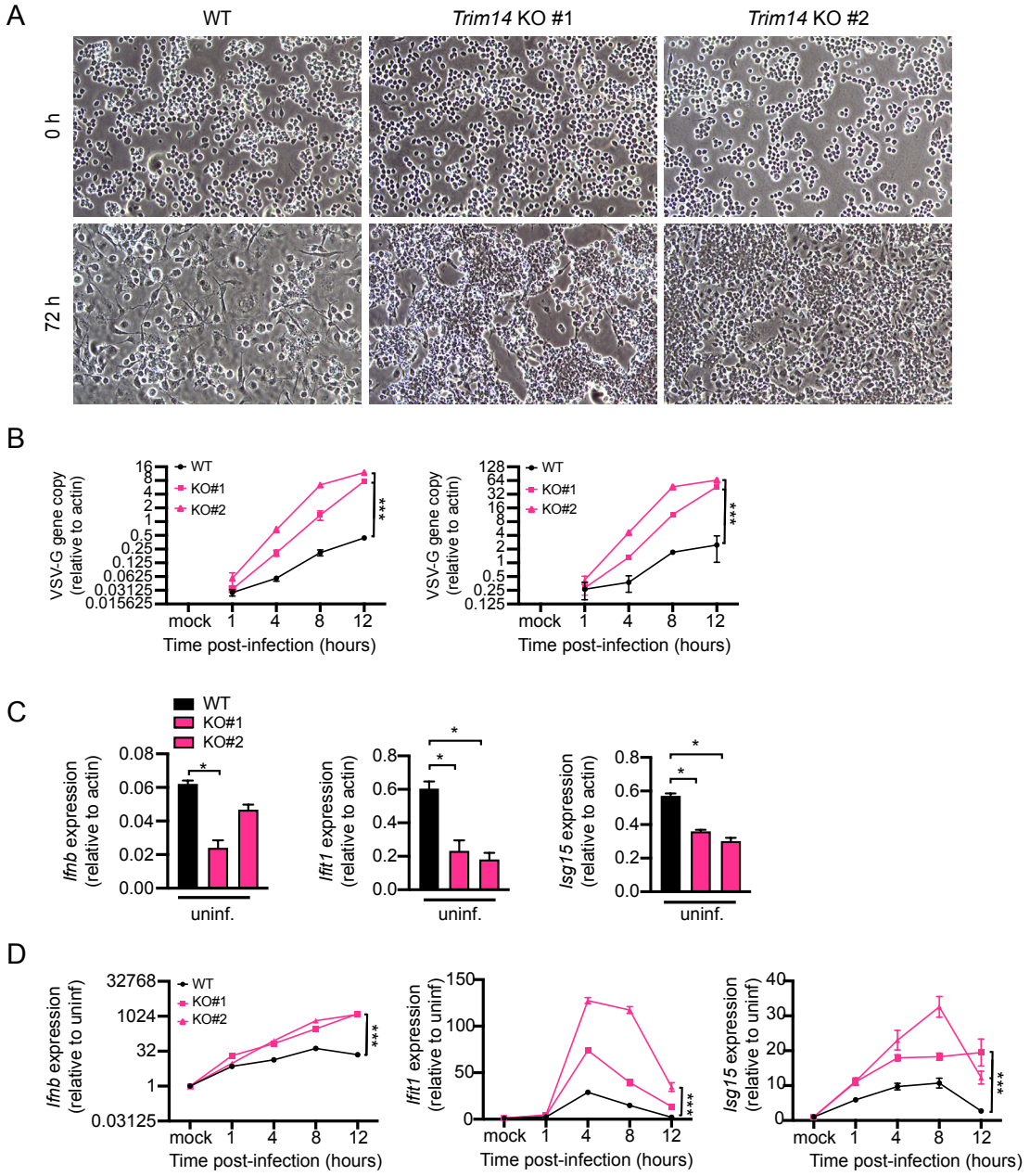

Figure S6. (A) Phase contrast images showing monolayers of WT and *Trim14* KO RAW 264.7 macrophages infected with Mtb *luxBCADE*. (B) Viral replication in WT and *Trim14* KO RAW 264.7 macrophages infected with VSV (MOI=1.0 or Mock infected) at 1h, 4h, 8h and 12h post-infection. (C) RT-qPCR of transcript levels in WT and Trim14 KO RAW 264.7 macrophages (D) RT-qPCR of transcript levels in WT and Trim14 KO RAW 264.7 macrophages infected with VSV (MOI=1.0 or Mock infected) at 1h, 4h, 8h and 12h post-infection.